REAL-SPACE ELECTRONIC STRUCTURE CALCULATIONS FOR NANOSCALE SYSTEMS

Tuomas Torsti

Laboratory of Physics
Helsinki University of Technology

Fysiikan laboratorio
Teknillinen korkeakoulu

DISSERTATION 121 (2003)

REAL-SPACE ELECTRONIC STRUCTURE CALCULATIONS FOR NANOSCALE SYSTEMS

Tuomas Torsti

Laboratory of Physics
Helsinki University of Technology
Espoo, Finland

Dissertation for the degree of Doctor of Science in Technology to be presented with due permission of the Department of Engineering Physics and Mathematics, Helsinki University of Technology for public examination and debate in Auditorium F1 at Helsinki University of Technology (Espoo, Finland) on the 27th of May, 2003, at 12 o'clock noon.

Dissertations of Laboratory of Physics, Helsinki University of Technology
ISSN 1455-1802

Dissertation 121 (2003):
Tuomas Torsti: Real-space electronic structure calculations
for nanoscale systems
ISBN 951-22-6469-2 (print)
ISBN 951-22-6470-6 (electronic)

PICASET OY
HELSINKI 2003

To Kerttu and Valtteri

HELSINKI UNIVERSITY OF TECHNOLOGY P.O. BOX 1000, FIN-02015 HUT http://www.hut.fi	ABSTRACT OF DOCTORAL DISSERTATION

Author Tuomas Torsti

Name of the dissertation

Real-space electronic structure calculations for nanoscale systems

Date of manuscript 8.5.2003	Date of the dissertation 27.5.2003
☐ Monograph	☑ Article dissertation (summary + original articles)

Department	Department of Engineering Physics and Mathematics
Laboratory	Laboratory of Physics
Field of research	Computational Condensed Matter Physics
Opponent(s)	Prof. Karsten W. Jacobsen
Supervisor	Academy Prof. Risto Nieminen
(Instructor)	Prof. Martti Puska

Abstract

In this thesis, basic research focused on quantum systems relevant for the future nanotechnologies is presented. The research is modeling based on electronic structure calculations using the density-functional theory. For the solution of the ensuing Kohn-Sham equations, we have developed a new numerical scheme based on the Rayleigh quotient multigrid method. While an important part of the thesis is formed by software development for three-dimensional first-principles real-space electronic structure calculations, we use axially symmetric model systems in the study of nanostructures. This approximation reduces the computational demands and allows studies of rather large nanoscale systems encompassing hundreds or thousands of electrons. In addition, by restricting the geometry to the axial symmetry and resorting to jellium models, many random effects related to the detailed ionic structure are absent, and the relevant physics is easier to extract from the simulations.

Nanowires can be considered as the ultimate conductors in which the atomistic confinement of electrons perpendicular to the wire and the atomistic length of the wire lead to quantum mechanical effects in cohesive and transport properties. The breaking process of a nanowire is studied using the ultimate jellium model, in which the positive background charge compensates in every point the electronic charge. Thereby, the shape of the narrowing constriction is free to vary so that the total energy is minimized. The prospect of molecular electronics is to use single molecules as circuit components. The electronic transport in atomic chains of a few Na atoms between cone-shaped leads is investigated in the thesis. Electrons residing in a Na island on the Cu(111) surface form a quantum dot system, in which the quantum mechanical confinement in all directions determines the electronic properties. We have developed a simple jellium model system which reproduces the characteristics of the confined electron states seen in scanning tunneling microscope experiments.

Keywords electronic structure, density-functional theory, multigrid method, parallel computing, nanowire, quantum dot

UDC	Number of pages 58 + 40
ISBN (printed) 951-22-6469-2 / 952-9821-85-9	ISBN (pdf)
ISBN (others) 951-22-6470-6	ISSN 1455-1802 / 0787-7498

Publisher Laboratory of Physics, Helsinki University of Technology / CSC - Scientific Computing Ltd.

Print distribution

☑ The dissertation can be read at http://lib.hut.fi/Diss/

Preface

This thesis has been prepared during the years 1999-2003, mainly in the Computational Condensed Matter and Complex Materials Group (COMP) in the Laboratory of Physics of the Helsinki University of Technology. In April 2002, CSC – Scientific Computing Ltd. and COMP started a collaborative project MIKA (Multigrid Instead of K-spAce) for development and application of real-space methods for electronic structure calculations. As a project manager of the MIKA-project, I have been employed by CSC during the final stage of the work.

I would like to thank my supervisor Academy Prof. Risto Nieminen for the opportunity to work in his excellent research group and also for encouraging me to work with first real-space first-principles methods and then axially symmetric models for nanowires in the early stage of this project, thereby catalyzing the birth of a program development effort with surprisingly large proportions. My deepest gratitude, however, is due to my advisor, Prof. Martti Puska whose guidance and collaboration has been of crucial importance in all stages of this work. I would also like to thank Paula Havu, Mika Heiskanen, Janne Ignatius, Vanja Lindberg, Mikko Lyly, Eduardo Ogando, Sampsa Riikonen, Juha Ruokolainen, Prof. Bo Hellsing and Prof. Nerea Zabala for collaboration in both published and unpublished work, and all the people working in the Laboratory of Physics and at CSC for creating pleasant working atmospheres.

I acknowledge financial support from Vilho, Yrjö and Kalle Väisälä foundation and the generous computer resources from CSC. I am grateful to CSC, my current employer, for providing me with the opportunity to take my time during the final stage of this thesis project, although it took a little longer than I first estimated.

Finally, I want to thank my wife Marjukka for support and my children Kerttu and Valtteri for reminding me from time to time that computational physics is not the only important thing in life.

Espoo, March 2003

Tuomas Torsti

Contents

List of publications

This thesis consists of an overview and the following publications:

I M. Heiskanen, T. Torsti, M. J. Puska, and R. M. Nieminen, *Multigrid method for electronic structure calculations*, Phys. Rev. B **63**, 245106 (2001).

II T. Torsti, M. Heiskanen, M. J. Puska, and R. M. Nieminen, *MIKA: a multigrid-based program package for electronic structure calculations*, Int. J. Quantum Chem. **91**, 171 (2003).

III P. Havu, T. Torsti, M. J. Puska, and R. M. Nieminen, *Conductance oscillations in metallic nanocontacts*, Phys. Rev. B **66**, 075401 (2002).

IV E. Ogando, T. Torsti, M. J. Puska, and N. Zabala, *Electronic resonance states in nanowires during the breaking process simulated with the ultimate jellium model*, Phys. Rev. B **67**, 075417 (2003).

V T. Torsti, V. Lindberg, M. J. Puska, and B. Hellsing, *Model study of adsorbed metallic quantum dots: Na on Cu(111)*, Phys. Rev. B **66**, 235420 (2002).

The author has had an active role in all the phases of the research reported in this thesis. He has been responsible for developing the computer programs for real-space pseudopotential calculations in three dimensions, reported in Publications I and II. He has implemented the numerical multigrid methods in axial symmetry as well as the versatile axially symmetric real-space pseudopotential/jellium code that has been applied for various nanostructure studies in Publications III, IV and V. He has had the main responsibility for the calculations reported in Publications I and V, as well as for the writing of Publications II and V. He has contributed actively to the planning, calculations and writing of Publications III and IV.

1 Introduction

Miniaturization has been the key ingredient for the rapid advance of the electronic technology. Today, the feature sizes in integrated circuits are of the order of 100 nm. In the near future the ultimate limit set by the atomic scale of 1 nm will be approached. But already before that the technology based on classical electron physics will move over to the domain where the principles of quantum mechanics have to be taken into account. This domain is referred to as nanotechnology.

In this thesis, basic research focused on quantum systems relevant for the future nanotechnologies is performed. Nanowires can be considered as the ultimate conductors in which the atomistic confinement of electrons perpendicular to the wire and the atomistic length of the wire lead to quantum mechanical effects in cohesive and transport properties. Electrons residing in a Na island on the Cu(111) surface form a quantum dot system, in which the quantum-mechanical confinement in all directions determines the electronic properties. The research is modeling based on electronic structure calculations using the density-functional theory. For the solution of the ensuing Kohn-Sham equations, we have developed a new numerical scheme based on the Rayleigh quotient multigrid method (RQMG), described in Publications I and II.

Conductance properties of chains consisting of a few Na atoms sandwiched between two metallic leads are examined in Publication III. We find that the conductance depends in an oscillatory manner on the number of atoms in the chain. In addition, we show that the shape of the contact leads has an important effect on the conductance. Cohesive and conducting properties of a nanocontact during the breaking process are studied in Publication IV using a model system, which highlights the effects of the electronic structure, ignoring the evolution of the detailed ionic configuration during the breaking process. Together with atomistic simulations and experiments, our model provides complementary insight into cohesive properties of nanowires. Finally, in Publication V, we develop a model system for adsorbed Na quantum dots on the Cu(111) surface. The electronic properties obtained can be quantitatively compared with scanning tunneling microscope measurements. In the future, our goal is to apply this model to study the reactivity of quantum dots, i.e. how different parameters as the size, shape and composition of the quantum dot may influence its ability to promote or prevent molecular dissociation or adsorption. The listed parameters control the

local electronic structure which in turn determines the scenario of an approaching gas phase molecule. This rather new field of surface physics is often referred to as nano-catalysis.

The computational framework for our nanostructure studies consists of the application of the Kohn-Sham scheme of density-functional theory in axial symmetry. We have chosen the axially symmetric approach, since this approximation reduces the computational demands and allows us to study rather large systems encompassing hundreds (Publications III and IV) and even thousands (Publication V) of electrons. In addition, by restricting the geometry to the axial symmetry and resorting to "jellium" models, we remove many random effects related to the detailed and uninteresting atomic structure from the model, and the relevant physics becomes more transparent in the simulations. In addition, it is particularly straightforward to exploit massively parallel computer architectures in the solution of the axially symmetric Kohn-Sham equations.

The RQMG-method reported in Publications I and II is a central ingredient in the numerical methodology used in our axially symmetric implementation of the Kohn-Sham scheme. Another motivation for developing the RQMG-method is for future applications in large-scale symmetry unrestricted atomistic real-space electronic structure calculations. For such calculations, plane-wave pseudopotential methods are nowadays routinely used. However, there are several aspects favoring the use of real-space methods. Therefore, in a second thread of this thesis project, the author has contributed to several key steps towards applications of the RQMG-method in atomistic calculations, involving e.g. structural relaxation of defects in semiconductors.

During this work, the Computational Condensed Matter and Complex Materials Group (COMP) of the Laboratory of Physics of the Helsinki University of Technology and CSC – Scientific Computing Ltd. have started a collaborative project called MIKA (Multigrid Instead of the K-spAce) towards the development and application of real-space methods in electronic structure calculations. The author has been appointed as the project manager of the MIKA-project. One of the first fruits of this collaboration has been the realization of the fact that the finite-element method and Krylov subspace techniques as implemented within the program package Elmer, developed at CSC, can be quite readily applied to electronic structure calculations. The finite-element approach has certain strengths, notably the adaptability of the mesh, that are absent from our current finite-difference

implementation of the RQMG-method. We expect, that the combination of the experience with the RQMG-method and electronic structure calculations gathered at COMP and the expertise on finite-element methods available at CSC will give rise to further improvements in the efficiency and accuracy of our numerical methods.

2 Electronic structure calculations

The goal of computational materials science and also that of modeling of nanoscale manmade structures is to calculate from first principles various physical and chemical properties. These properties can in principle be calculated by solving for the many-body wave function, which is a function of both the electronic and nuclear degrees of freedom. Due to the large difference in mass between the electrons and the nuclei, the electronic and nuclear degrees of freedom may be decoupled. In the Born-Oppenheimer approximation, the nuclei are assumed to be fixed in space, and the antisymmetric wave function $\Psi(\mathbf{r_1}, \ldots, \mathbf{r_N})$ depending on the spatial electronic coordinates[1] is obtained from the Schrödinger equation

$$\hat{H}\Psi(\mathbf{r_1}, \ldots, \mathbf{r_N}) = E\Psi(\mathbf{r_1}, \ldots, \mathbf{r_N}), \tag{1}$$

$$\hat{H} = -\frac{1}{2}\sum_i \nabla_i^2 - \sum_i V_{\text{ext}}(\mathbf{r}_i) + \sum_{i<j} \frac{1}{|\mathbf{r}_i - \mathbf{r}_j|}. \tag{2}$$

The external potential may be caused by the nuclei as discussed above

$$V_{\text{ext}} = \sum_I \frac{Z_I}{|\mathbf{r}_i - \mathbf{R}_I|}, \tag{3}$$

or it may have some other form. In Eqs. (1-3), $\mathbf{r}_i$ refers to the position of electron i and Z_I and R_I to the charge and position of nucleus I, respectively. Eq. (1) can in practice be numerically solved only in the case of a few electrons. Above, and throughout this thesis, atomic units where $e = \hbar = m_e = 1$, are used. The energy unit is thus 1 Hartree (Ha) $\approx$ 27.2 eV.

2.1 Density-functional theory

In the density functional theory [1–5], the many-body problem is approached from a different viewpoint. Instead of the many-body wave function Ψ, the central quantity is the electron density $n(\mathbf{r})$. The number of degrees of freedom is reduced from $3N$ to 3, and the problem is drastically simplified. This idea dates back to the early works of Thomas [6] and Fermi [7].

[1]For simplicity, we neglect the electron spin.

A formal justification for this replacement is provided by the Hohenberg-Kohn (HK) theorems [8]. The first HK theorem states that the ground state electron density determines the external potential V_{ext} within an additive constant. Since V_{ext} defines the Hamiltonian in Eq. (2), the electron density also defines the ground state wave function and hence all the ground state properties, including the ground state energy $E_0 = E[n_0]$. The second HK theorem associates a variational principle with the ground state energy: $E_0 = \min E[n]$, where the search is over V-representable densities that correspond to some external potential. A more general formulation of this theorem [9] expands the search over N-representable densities – the non-negative densities that integrate to N particles. This more general formulation of the HK-theorem is known as constrained search and states

$$E_0 = \min_{n(\mathbf{r})\to N} \left\{ \min_{\Psi\to n(\mathbf{r})} \langle\Psi|\, \hat{T} + \hat{V}_{e-e}\, |\Psi\rangle + \int d\mathbf{r} n(\mathbf{r}) V_{\text{ext}}(\mathbf{r}) \right\}. \tag{4}$$

$F[n] = \min_{\Psi\to n(\mathbf{r})} \langle\Psi|\, \hat{T} + \hat{V}_{e-e}\, |\Psi\rangle$ does not depend on the details of the external potential and is therefore a universal functional. A closed form for $F[n]$ is unfortunately not known.

Kohn and Sham [10] suggested to split $F[n]$ as follows,

$$F[n] = T_s[n] + \int d\mathbf{r} d\mathbf{r}' \frac{n(\mathbf{r})n(\mathbf{r}')}{|\mathbf{r}-\mathbf{r}'|} + E_{xc}[n], \tag{5}$$

where $T_s[n]$ is the kinetic energy of a reference system of noninteracting electrons with the density $n(\mathbf{r})$. All the many-body effects have now been hidden in the functional $E_{xc}[n]$. It may be instructive to list the three physical effects included in E_{xc}. First, a negative potential energy term is included (the exchange energy, tending to cancel part of the Hartree potential energy). This arises because the antisymmetry of the wave-function causes electrons of the same spin projection to avoid each other. Another negative potential energy term, the correlation potential energy, a further reduction of the Hartree potential energy, occurs because the Coulomb potential causes electrons of either spin to avoid each other. Finally E_{xc} encompasses a positive correlation contribution to the kinetic energy, an effect of the uncertainty and Pauli principles; mutual avoidance reduces the space available and hence raises the kinetic energy.

In practice, the Kohn-Sham scheme leads to the self-consistent solution of the N lowest eigenvalues ε_i and the corresponding single-particle wave

functions $\psi_i(\mathbf{r})$ of the coupled set of Kohn-Sham equations,

$$-\frac{1}{2}\nabla^2\psi_i(\mathbf{r}) + V_{\text{eff}}(\mathbf{r})\psi_i(\mathbf{r}) = \varepsilon_i\psi_i, \tag{6}$$

$$n(\mathbf{r}) = \sum_i^N |\psi_i(\mathbf{r})|^2, \tag{7}$$

$$V_{\text{eff}}(\mathbf{r}) = V_{\text{ext}}(\mathbf{r}) + V_{\text{H}}(\mathbf{r}) + V_{\text{xc}}(\mathbf{r}), \tag{8}$$

$$V_{\text{H}}(\mathbf{r}) = \int \frac{n(\mathbf{r}')}{|\mathbf{r}-\mathbf{r}'|} d\mathbf{r}', \tag{9}$$

$$V_{\text{xc}}(\mathbf{r}) = \frac{\delta E_{\text{xc}}[n(\mathbf{r})]}{\delta n(\mathbf{r})}. \tag{10}$$

The first equation (6) is a Schrödinger equation for non-interacting particles in an effective potential $V_{\text{eff}}(\mathbf{r})$. The electron density $n(\mathbf{r})$ is obtained from a sum over the N occupied states. The effective potential consists of an external potential $V_{\text{ext}}(\mathbf{r})$ due to ions (or nuclei in all-electron calculations), the Hartree potential $V_{\text{H}}(\mathbf{r})$ calculated from the electron density distribution, and the exchange-correlation potential $V_{\text{xc}}(\mathbf{r})$, which is obtained as a functional derivative of E_{xc}.

The simplest approximation for E_{xc} is the *local density approximation* (LDA) already suggested by Kohn and Sham in their original paper [10]. In this approximation, the properties of the homogeneous electron gas (EG) are extrapolated to inhomogeneous systems,

$$E_{xc}^{LDA} = \int d\mathbf{r} n(\mathbf{r}) \varepsilon_{xc}^{EG}(n(\mathbf{r})), \tag{11}$$

where $\varepsilon_{xc}^{EG}(n)$ denotes the exchange-correlation energy per electron of a uniform electron gas with density n. Using the results of quantum Monte-Carlo calculations for this system [11], accurate parametrizations have been derived [12–14]. From its definition, one would only expect the LDA to give accurate results for systems with slowly varying electron densities. However, for real systems, especially solids, where this condition is strongly violated, LDA is surprisingly accurate. However, LDA has limitations, especially for open systems like surfaces and molecules.

For more accurate description of such systems, exchange-correlation functionals involving, for example, the gradient of the electron density have

been developed. The first functional that falls into the class of *generalized gradient approximations* (GGA) was proposed by Perdew and Wang [15]. Also the BP86-functional, which is a combination of Beckes exchange functional B88 [16] and Perdew's correlation functional P86 [17] is widely used. Beckes three-parameter hybrid functional (B3LYP) [18, 19], a linear combination of Hartree-Fock and DFT energies, has been found in many situations to improve the energies of pure DFT functionals [20]. For more recent developments of GGA-functionals by Perdew *et al.*, the reader is referred to Refs. [21–23]. With the introduction of GGA-functionals, the accuracy of DFT for molecular systems has become competitive with more traditional quantum chemical formalisms, which aim at direct approximate solution of the many-body Schrödinger equation (Eq. 1), while the scaling of the computational cost of DFT with system size is more attractive.

2.2 Jellium models

The jellium model has long traditions in self-consistent electronic-structure calculations of systems that are nowadays often referred to as nanostructures, such as surfaces, vacancies and voids, atomic clusters, and nanowires. It simplifies the problem by replacing the discrete ions by a uniform rigid positive charge density background, which globally neutralizes the electron negative charge. The effective potential of the Kohn-Sham equations is written as

$$V_{\text{eff}} = \int \frac{n_-(r') - n_+(r')}{|r - r'|} dr' + V_{\text{xc}}[n_-(r)], \tag{12}$$

where the first term on the right-hand side includes the electron-electron and electron-positive background Coulomb interactions and the second term gives the exchange-correlation potential within the LDA.

2.2.1 Stabilized jellium

Different types of jellium approaches have been introduced. The simple jellium (SJ) model corresponding to Eq. (12) has the problem that there is only one equilibrium charge density, at $r_s \approx 4.18\ a_0$ ($n_- = 3/(4\pi r_s^3)$) corresponding approximately to the average conduction electron density in the Na metal. This means that for r_s values lower (higher) than $\sim$4.18 a_0, the jellium system tends to expand (compress). In the SJ-model the electron density has the same mean value as the positive background due to the

electrostatic forces. The SJ-model gives incorrect predictions of properties such as the cohesive energy, surface energy and bulk modulus, due to the tendency of the system to compress or expand. To improve the results, corrections can be added to the SJ-model [24], e.g. using the so-called stabilized jellium model [25] introduced by Perdew *et al.* [26] and Shore and Rose [27]. We have used the stabilized jellium model to describe conical Na leads in Publication III. In Publication V, we have used two slabs of simple jellium of different densities in our two-jellium model, which captures the essential physics of the adsorption system Na on Cu(111).

2.2.2 Ultimate jellium

In Publication IV, we have used the ultimate-jellium (UJ) model, the philosophy of which differs from the stabilized jellium model in that it does not try to correct the above-mentioned deficiencies of the SJ-model. The peculiarity of the UJ-model is that the positive charge background is allowed to relax. The UJ-model represents the ultimate limit in which the positive background can completely relax to have the same density as the electrons at every point, leading not only to global but also local neutralization. In this way, the Coulomb terms in the total energy and effective potential vanish. The total energy is then minimized in the interplay between the exchange-correlation and the kinetic energies. From the practical numerical point of view, the UJ-model has a gratifying property - the lack of Coulomb interactions and therefore the lack of the charge sloshing. The self-consistent iterations converge rapidly and the speed of convergence (in terms of the number of iterations) is independent of the system size.

One limitation of the UJ-model is that for an infinite system, as in the SJ-model, there is only one equilibrium charge density, at $r_s \approx 4.18\ a_0$. The absence of electrostatic potential disables the mechanism to keep the electrons at a given density, and inside the UJ the mean electron density becomes equal to the equilibrium density. Another property of the UJ-model, as a consequence of the absence of electrostatic potential, is that the shape of the electron density is to a large extent uncontrollable, and it evolves until the ground state is achieved. This property has been used to study the most favorable shapes of simple-metal atom clusters [28–30]. The realm of applications of the UJ-model may be extended by application of controlling restrictions, such as an external potential [31, 32]. Moreover, in Publication IV we have used, in order to model the cohesive properties of

nanowires, the conservation of certain symmetries and the conservation of the shape of the effective potential in certain parts of the system.

3 Real-space methods

The plane-wave pseudopotential method has proven to be an excellent computational tool for solving large-scale electronic structure problems in condensed-matter physics [33, 34]. Notable strengths of the method are the ability to use the fast Fourier transform for updating the Kohn-Sham equations, lack of dependence of the basis on atom positions, and the clear control of convergence with the cutoff energy determined by the shortest-wavelength mode. However, the method encounters difficulties in treating widely varying length scales. This issue is relevant for all-electron calculations, surfaces, clusters, and the hard pseudopotentials of first-row elements or transition metals, which vary rapidly near the nucleus. It is not necessary to use the supercell approximation, when treating clusters or molecules with real-space methods. However, it should be noted, that this is not necessary in the plane-wave methodology either. Barnett and Landman [35] have implemented a plane-wave scheme for isolated clusters.

Real-space approaches, where the basis functions are atom-centered or floating Gaussians or atomic orbitals, are very well established, and are used by the majority of the quantum-chemistry community as well as by an increasing number of condensed-matter physicists. A wide selection of well-established codes based on atom-centered basis functions is available, including e.g. Gaussian [36], Dmol [37], Adf [38], Turbomole [39], NWChem [40] and Siesta [41]. The basis sets used in these methods are smaller than in the plane-wave methods, but the magnitude of the related basis-set truncation error is more difficult to estimate.

Considerable effort has recently been focused also on developing "fully numerical" real-space methods [42], which permit systematic studies of convergence in the spirit of the plane-wave methods. These methods are based on finite elements [43–47], finite-difference discretizations [48–54] or wavelets [55]. Advantages of these approaches include the free choice of boundary conditions, allowing e.g. the treatment of finite and periodic systems with equal effort. Near-locality of the kinetic energy operator in real-space representations leads to simplicity in developing domain-decomposition parallel algorithms. In addition, it is possible to implement adaptive grid-refinement strategies to focus effort in spatial regions with large variations in the computed functions, for example near the nuclei. In finite-difference methods, the available strategies for mesh refinement include composite grids [56–58] and adaptive coordinates [54, 59]. In finite-element methods, on the

other hand, there is more freedom in the choice of the computational mesh. However, generating an optimal finite element mesh (or finite-difference composite grid) for a given problem is a nontrivial task [60–62], which either requires *a priori* knowledge of the spatial dependence of the required density of the mesh, or involves a repeated sequence of solving the problem in a given mesh, making an *a posteriori* error estimation and then remeshing. Representations on real-space grids allow also the use of multigrid (MG) algorithms with their excellent convergence characteristics and scaling properties [63, 64]. A real-space formulation is also often used in efficient implementations of $O(N)$ methods for electronic-structure calculations, in which the computational work required scales linearly with the number of atoms [65, 66].

Among the pioneers of real-space methods for molecular systems were A. D. Becke [67, 68] and Pyykkö *et al.* [69–71], who made highly accurate fully numerical all-electron real-space calculations for diatomic molecules, employing the prolate spheroidal coordinate system. In the axial symmetry of diatomic molecules, the azimuthal dependence of the single-particle functions can be treated analytically and the ensuing numerical problem is two-dimensional. Their approach for diatomic molecules is very similar to our more general method for axially symmetric systems, described in Sec. 4. Besides density-functional theory, Pyykkö *et al.* applied their fully numerical approach to other quantum chemical models such as Hartree-Fock, MCSCF, and relativistic DFT calculations [69].

Several approaches employing the multigrid idea within electronic structure calculations have appeared during the last decade [50–53, 66, 72]. The main idea of multigrid methods is that they avoid the critical slowing-down (CSD) phenomenon occuring when a partial differential equation discretized on a real-space grid is solved with a simple relaxation method such as the Gauss-Seidel method. The discretized operators use information from a rather localized region of the grid at a time. Therefore the high-frequency error of the length scale of the grid spacing is reduced very rapidly in the relaxation. However, once the high-frequency error has effectively been removed, the slow convergence of the low-frequency components dominates the overall error reduction rate [63], i.e. CSD occurs. In multigrid methods one stops the relaxation on a given (fine) grid before CSD sets in and transfers the equation to a coarser grid (the so-called restriction operation) where the low-frequency components can be solved more efficiently. On the coarsest grid the problem is solved exactly or as accurately as possible, after which one

interpolates (the so-called prolongation operation) the correction to finer grids, performing simultaneously relaxations in order to remove the high-frequency errors introduced in the interpolation. Refs. [73, 74] are classical textbooks on multigrid methods. Introductory material can be found in the recently appeared second edition of the Multigrid tutorial by W. L. Briggs *et al.* [75].

The full-approximation storage method [63] (FAS) is a standard recipe for nonlinear problems. Beck *et al.* [53, 76] have applied the FAS eigensolver of Brandt *et al.* [64] for electronic structure calculations of small molecules. Costiner and Ta'asan [77, 78] have made several technical improvements to overcome various obstacles related to the application of the FAS-method in electronic structure calculations. It has also been noted [78, 79], that the FAS-scheme, applicable to nonlinear systems of equations, can be directly applied to the nonlinear Kohn-Sham problem, bypassing the self-consistency iterations. However, according to the author's knowledge, none of these methods are yet routinely applied in large-scale electronic structure calculations. When many eigenfunctions are solved simultaneously, the FAS methods may suffer from problems with representing the eigenfunctions accurately on the coarse levels, limiting the number of levels that can be used.

Briggs *et al.* [50, 72] apply a linearized multigrid algorithm, where the potential does not appear at all in the coarse-grid equations. Thus, on the coarse grids, they solve for a Poisson equation, obtaining some acceleration for the convergence of the Schrödinger equation, accurately discretized on the fine level only. Although this scheme clearly does not reach optimal convergence speeds, it has been used on a routine basis for several years in electronic structure calculations.

Multigrid methods are not the only efficient solvers for the matrix eigenproblems arising from the finite-difference or finite-element discretization of the Kohn-Sham equations. Chelikowsky *et al.* [48, 80–82] have succesfully applied iterative diagonalization schemes based on preconditioned Krylov techniques, such as the Lanczos method [83]. However, even for such methods, multigrid methods may have relevance as the optimal preconditioners for the ensuing linear systems of equations, when the system size is large.

3.1 The Rayleigh quotient multigrid method

In order to avoid the coarse grid representation problems we have developed a generalization of the so-called Rayleigh quotient multigrid method (RQMG) introduced by Mandel and McCormick [84]. Our generalization is presented in Publication I. In this method the coarse grid relaxation passes are performed so that the Rayleigh quotient calculated on the *fine* grid will be minimized. In this way there is no requirement for the solution to be well represented on a coarse grid and the coarse grid representation problem is avoided. Mandel and McCormick [84] introduced the method for the solution of the eigenpair corresponding to the lowest eigenvalue. We have generalized it to the simultaneous solution of a desired number of lowest eigenenergy states by developing a scheme which keeps the eigenstates separated by the use of a penalty functional, Gram-Schmidt orthogonalization, and subspace rotations.

A basic ingredient of our scheme is a very simple relaxation method called coordinate relaxation [85]. Coordinate relaxation is a method of solving the discretized eigenproblem

$$Hu = \lambda Bu \tag{13}$$

by minimizing the Rayleigh quotient

$$\frac{\langle u|H|u\rangle}{\langle u|B|u\rangle}. \tag{14}$$

Above, H and B are matrix operators chosen so that the Schrödinger equation discretized on a real-space point grid with spacing h is satisfied to a chosen order $O(h^n)$. In Eq. (14) u is a vector, containing the values of the Kohn-Sham orbitals at the grid points. In the relaxation method, the current estimate u is replaced by $u' = u + \alpha d$, where the search vector d is simply chosen to be unity in one grid point and to vanish in all other points, and α is chosen to minimize the Rayleigh quotient. This leads to a simple quadratic equation for α. For complex eigenfunctions it is possible to either solve a remarkably complicated coupled pair of quadratic equations for the real and imaginary parts of α, or to sequentially apply separate coordinate relaxation steps for the real and imaginary parts. A complete coordinate relaxation pass is then obtained by performing the minimization at each point in turn and these passes can be repeated until the lowest state is found with desired accuracy.

Naturally, also the coordinate relaxation suffers from CSD because of the use of local information only in updating u in a certain point. In order to avoid it one applies the multigrid idea. In the multigrid scheme by Mandel and McCormick [84] the crucial point is that *coarse* grid coordinate relaxation passes are performed so that the Rayleigh quotient calculated on the *fine* grid will be minimized. In this way there is no requirement for the solution to be well represented on a coarse grid. In practice, a coarse grid search substitutes the fine grid solution by

$$u'_f = u_f + \alpha I_c^f e_c, \tag{15}$$

where the subscripts f and c stand for the fine and coarse grids, respectively, and I_c^f a prolongation operator interpolating the coarse grid vector to the fine grid. The Rayleigh quotient to be minimized is then

$$\frac{\langle u_f + \alpha I_c^f d_c | H_f | u_f + \alpha I_c^f d_c \rangle}{\langle u_f + \alpha I_c^f d_c | B_f | u_f + \alpha I_c^f d_c \rangle} = \frac{\langle u_f | H_f u_f \rangle + 2\alpha \langle I_f^c H_f u_f | d_c \rangle + \alpha^2 \langle d_c | H_c d_c \rangle}{\langle u_f | B_f u_f \rangle + 2\alpha \langle I_f^c B_f u_f | d_c \rangle + \alpha^2 \langle d_c | B_c d_c \rangle}. \tag{16}$$

The second form is obtained by relating the coarse grid operators, H_c and B_c, with the fine grid ones, H_f and B_f, by the Galerkin condition

$$H_c = I_f^c H_f I_c^f; \quad B_c = I_f^c B_f I_c^f; \quad I_f^c = \left(I_c^f\right)^T. \tag{17}$$

Note, however, that the Galerkin condition is not satisfied in our actual implementation – instead we discretize the original equation separately on each grid to obtain H_c and B_c [discretization coarse grid approximation (DCA)].

The key point to note is that when $H_f u_f$ and $B_f u_f$ are provided from the fine grid to the coarse grid, the remaining integrals can be calculated on the coarse grid itself. Thus one really applies coordinate relaxation on the coarse grids to minimize the *fine level* Rayleigh quotient. This is a major departure from the earlier methods, which to some extent rely on the ability to represent the solution of some coarse grid equation on the coarse grid itself. Here, on the other hand, one can calculate the *exact* change in the Rayleigh quotient due to *any* coarse grid change, no matter how coarse the grid itself is. There is no equation whose solution would have to be representable.

Next we consider the generalization of the RQMG method to the simultaneous solution of several (N) mutually orthogonal eigenpairs. The separation

of the different states is divided into two or three subtasks. First, in order to make the coarse grid relaxations converge towards the desired state we apply a penalty functional scheme. Given the current approximations for the k lowest eigenfunctions, the next lowest, $(k+1)$'th state is updated by minimizing the functional

$$\frac{\langle u_{k+1}|H|u_{k+1}\rangle}{\langle u_{k+1}|B|u_{k+1}\rangle} + \sum_{i=1}^{k} q_i \frac{|\langle u_i|u_{k+1}\rangle|^2}{\langle u_i|u_i\rangle \cdot \langle u_{k+1}|u_{k+1}\rangle}. \tag{18}$$

The modulus of the overlap integral in the penalty term is squared to make the penalty positive definite. The denominator is required to make the functional independent of the norms of u_i, $i = 1 \ldots k+1$. The minimization of this functional is equivalent to imposing the orthonormality constraints against the lower k states, when $q_i \to \infty$. By increasing the shifts q_i any desired accuracy can be obtained, but in order to obtain a computationally efficient algorithm a reasonable finite value should be used, for example

$$q_i = (\lambda_{k+1} - \lambda_i) + \mathrm{Q}, \tag{19}$$

where Q is a sufficiently large positive constant. In our calculations we have used the value $Q = 2$ Ha.

The substitution (15) is introduced in the functional (18) and the minimization with respect to α leads again to a quadratic equation. This time the coefficients contain terms due to the penalty part.

While the penalty functional keeps the states separated on the coarse levels, we apply a simple relaxation method (Gauss-Seidel) on the finest level. The Gauss-Seidel method converges to the nearest eigenvalue, so ideally no additional orthogonalizations would be needed. In practice, however, we use Gram-Schmidt orthogonalizations and subspace rotations. However, the number of fine grid orthogonalizations remains small, for example, in comparison with the conjugate gradient search of eigenpairs employing only the finest grid [49].

3.2 Obtaining self-consistency

The Kohn-Sham equations have to be solved self-consistently, i.e. the wave functions solved from the single-particle equation determine via the density (solution of the Poisson equation and the calculation of the exchange-correlation potential) the effective potential for which they should again be

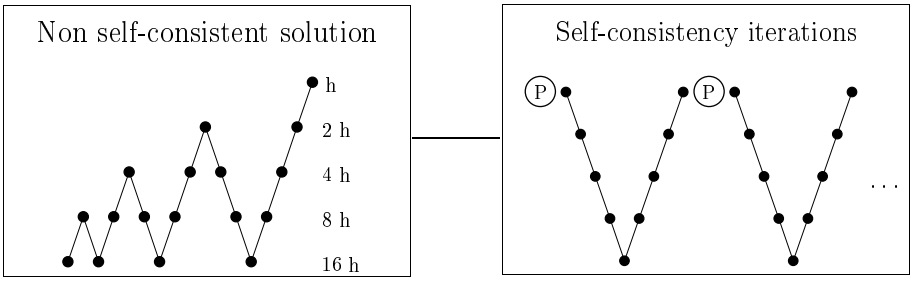

Figure 1: Strategy of self-consistency iterations. First, the Kohn-Sham orbitals are solved nonselfconsistently using the full multigrid method in the initial potential corresponding to the superposition of pseudoatoms. Then the effective potential is updated (this is denoted by P in the figure). The potential update amounts to calculation of the new electron density, the solution of the Poisson equation and calculation of the new exchange correlation potential. Next the Kohn-Sham orbitals are updated by one V-cycle. These two steps are repeated until self-consistency has been reached.

solved. To approach this self-consistency we apply an optimized strategy so that numerical accuracy of the Kohn-Sham orbitals and that of the potential increase in balance, enabling the most efficient convergence. Our strategy consisting of sequential updates for the Kohn-Sham orbitals and the potential during the self-consistency iterations is illustrated in Fig. 1.

It is well known that using the output potential of an iteration step as a new input for the subsequent iteration might lead to instabilities in the iteration process. In fact the source of this instability can be traced to the long range of the Coulomb potential and is particularly severe for large systems. An input potential which deviates from the self-consistent potential contains spurious Coulomb contributions which cause the electronic charge to overshoot from iteration to iteration. This phenomenon is called charge sloshing. To damp the charge density oscillations, we have applied the conventional mixing scheme, where the new effective potential $V_{\rm in}^{n+1}$ is obtained from the input and output potentials of the previous iteration as

$$V_{\rm in}^{(n+1)} = (1-\kappa)V_{\rm in}^{(n)} + \kappa V_{\rm out}^{(n)}, \qquad 0 < \kappa \leq 1. \tag{20}$$

In our test calculations for the CO_2-molecule and bulk Si reported in Publication I, we obtain rapid convergence with $\kappa \approx 0.5$. Later, however, we have encountered systems, where very small values for κ are necessary to

avoid divergence, and hundreds of iterations are needed to obtain convergence. Therefore, it is important to implement a more sophisticated mixing scheme in the future [86–93]. One idea [86–88] which we have already implemented, is to use, instead of the Poisson equation, the following recursive modified Helmholz equation

$$(\nabla^2 - k^2)V_C^{(n)}(\mathbf{r}) = -4\pi\left(\rho(\mathbf{r}) + \frac{k^2}{4\pi}V_C^{(n-1)}(\mathbf{r})\right), \tag{21}$$

the solution of which is

$$V_C^{(n)} = \int \frac{\exp(-k|\mathbf{r}-\mathbf{r}'|)}{|\mathbf{r}-\mathbf{r}'|}\left(\rho(\mathbf{r}) + \frac{k^2}{4\pi}V_C^{(n-1)}(\mathbf{r})\right). \tag{22}$$

It can be seen that at convergence this scheme will give the correct Coulomb potential. In addition, the exponential kernel in Eq. (22) essentially eliminates contributions from $\rho(\mathbf{r})$ outside a sphere of radius equal to $1/k$. Thus this scheme eliminates problems due to long-range Coulomb interactions of spurious charge oscillations. In plane-wave methods, the related scheme known as the Kerker mixing [89] is widely used.

3.3 MIKA – a program package and a project

The RQMG-method described above has been harnessed for use in several applications, i.e. computer programs devoted to the modelling of specific classes of physical systems. It is convenient to refer to the collection of applications and the numerical implementation of the RQMG-method collectively with a single name. Thus the name Mika (Multigrid Instead of K-spAce) was coined for the program package (Publication II). In the middle panel of Fig. 2, the main components of the program package are shown. The numerical solvers for the Schrödinger and Poisson equations are collected in the subroutine library `MGLIB`. The first applications of the atomistic, three-dimensional real-space pseudopotential method as implemented in `rspace` were discussed in Sec. 3.1. In addition, some recent developments of `rspace` are briefly discussed is Sec. 3.4. In the left panel of Fig. 2 an example from an archetypal application of electronic structure calculations is shown – the electron density corresponding to the so-called deep states in the neutral, ideal (no ion-relaxation) vacancy in Si.

Special software, the program `cyl2`, has been written for electronic structure calculations in axial symmetry. Applications to diverse nanophysics problems (Publications III,IV,V) are discussed in Sec. 4. Quantum dots and

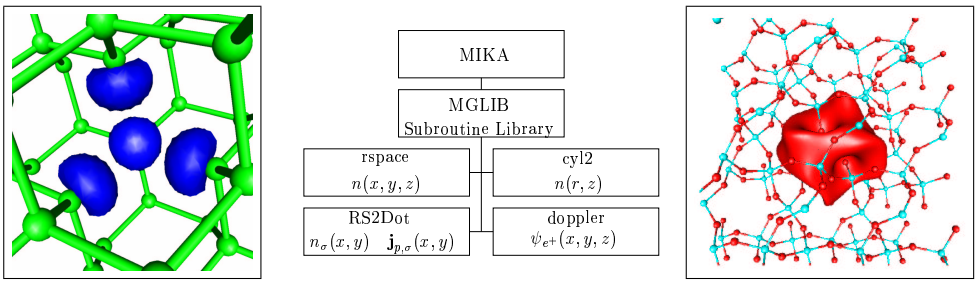

Figure 2: Left panel: electron density isosurface corresponding to the deep states localized at the neutral, ideal (no ion relaxation) vacancy in bulk Si. Middle panel: Schematic illustration of the software comprising the MIKA-package. Right panel: Isosurface of the positron state localized at a Si vacancy in SiO_2.

quantum dot molecules in two-dimensional electron gas are being studied using `RS2Dot` [94–96] – a code designed for electronic structure calculations in two dimensions. Software for studying positron annihilation in solids has been developed earlier [97], and referred collectively with the name `doppler`. In these programs, a key ingredient is the numerical solver of the positron wave function. The RQMG-method has replaced the former, less efficient, conjugate-gradient method [49] in this application as well. As an example of positron calculations, the right panel of Fig. 2 shows a positron wave function localized in the Si-vacancy in SiO_2. It should be added here, that a one-dimensional version of the RQMG-method has been implemented as well, and applied in the calculation of the influence of electron-electron interactions on the supercurrent in superconductor-normal metal-superconductor (SNS) structures [98].

In addition to the program package described above, the name MIKA has been adopted for a collaborative project, started in 2002 by CSC and COMP. In addition to COMP, three other Finnish research groups have expressed their interest in joining this collaborative effort towards development and application of real-space methods for electronic structure.

3.4 Work in progress

Recently [99], several steps were taken to develop further the three-dimensional RQMG-based pseudopotential code `rspace`. The program was parallelized over **k**-points and real-space domains. The time-saving double-grid

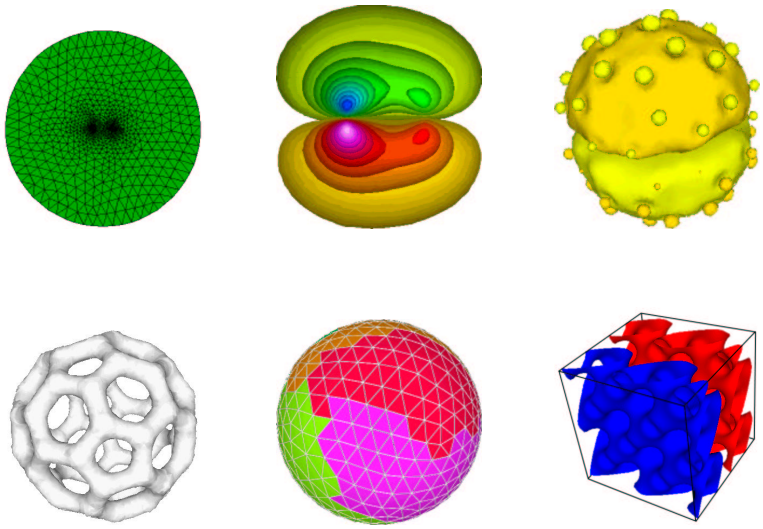

Figure 3: Some electronic structure calculations using ELMER. All-electron calculations for the molecules CO and C_{60} were done. Schrödinger equation was solved in a periodic potential corresponding to bulk silicon. See also the text.

method of Ono and Hirose [100] was implemented. The Hellman-Feynman forces [101] and relaxation of the ionic coordinates using the Broyden--Fletcher-Goldfarb-Shanno (BFGS) algorithm [102–106] were implemented. With the aim of relaxing structures of positron-decorated defects in solids, the calculation of positron-induced ionic forces was implemented. In practice, this was realized by making a subroutine call from `rspace` to the well-established implementation of the atomic-superposition method [97] within `doppler`. A preliminary relaxation of the positron-decorated silicon vacancy was done using the 63-atom supercell. The Brillouin-zone was sampled using the Γ-point only. The results of this calculation will be reported elsewhere, after a careful review of the details of the implementation and proper convergence of the calculation. It should be noted here that Probert *et al.* [107] have recently shown that accurate calculations for the neutral vacancy in Si require special care in the choice of the supercell and **k**-point sampling. The same may be true for the positron decorated vacancy in Si.

At CSC, a general purpose program package ELMER for partial differential equations has been developed during the last decade. In ELMER, the equations are discretized using the finite-element method [108, 109] on arbitrary meshes, which can be generated to match the demands of the problem to

be solved.

A natural first step in the collaboration of COMP and CSC in the MIKA-project was to assess the feasibility of using ELMER for electronic structure calculations. Fig. 3 illustrates three successful test cases, indicating the feasibility of ELMER in electronic structure calculations. The most important strength of ELMER in comparison to `rspace` is the flexibility of the finite-element mesh. Although equivalent adaptivity can be reached in finite-difference methods through the use of composite grids [56–58], the related technical difficulties may be sufficient to suppress their actual implementation within the MIKA-package. Nonuniform meshes allow the treatment of systems with multiple length scales. Such systems are quite common in electronic structure calculations – examples are all-electron calculations, hard pseudopotentials and surfaces. The need for accurate treatment of such systems is one of the main reasons for developing real-space methods.

As the first self-consistent calculation within the local-density approximation of the density-functional theory using ELMER, an all-electron calculation for the carbon monoxide molecule was done. The top left panel of Fig. 3 illustrates the selected finite-element mesh. Since the divergent $(1/r)$ potential has to be represented on the mesh, a very fine mesh is used in the immediate neighbourhood of the singularity. The Lanczos method [83] with shift-and-invert preconditioning [110] was used to solve the resulting eigenproblem with high accuracy at each iteration of the self-consistency cycle. The initial guess for the effective potential was the sum of the bare nuclear potentials. Although a very small value for κ in Eq. (20) was needed in the first few SC-iterations, tight convergence in less than 20 iterations was obtained by increasing κ in an *ad hoc* manner during the self-consistency cycle. In the middle panel of the upper row of Fig. 3 a contour plot of a single-particle wave function provided by the Kohn-Sham scheme is shown. Also larger molecules can be treated using this all-electron scheme within ELMER. The top right panel of Fig. 3 shows a selected orbital from an all-electron calculation of the C_{60}-molecule. The lower left panel illustrates the electron density of C_{60}, obtained from a parallel calculation involving eight processors and 4×10^5 degrees of freedom. The lower middle panel of Fig. 3 illustrates the partitioning of the mesh that was used – domains with different colours were mapped to different processors. Periodic boundary conditions were implemented within ELMER, and in order to compare the computational efficiency of the RQMG method and the Lanczos method, the Schrödinger equation was solved (i.e. a non-self-consistent calculation

was done) in a periodic potential corresponding to bulk silicon using both methods. A uniform grid consisting of 32^3 points was used in the 64-atom supercell. The computational efficiencies of the two methods were similar – an accuracy of 10^{-5} eV (or better) in the eigenvalues was obtained in 900 seconds. The lower right panel of Fig. 3 illustrates a selected eigenfunction from this periodic test case.

There is plenty of room for improvement in the computational efficiency of our finite-element scheme. While the highly accurate all-electron calculation for C_{60} with 4×10^5 degrees of freedom required 48 hours of wall-clock time when calculated using 8 processors on an IBM eServer Cluster 1600, a pseudopotential calculation using `rspace` on 48^3 grid required only 15 hours on a single processor. Implementing pseudopotentials, higher-order elements and possibly the RQMG-method within Elmer will improve the efficiency. The high-order finite-difference approach allows the use of coarse grids in pseudopotential calculations, but the price to be paid is lower accuracy due to the coarse sampling of the potential [48]. However, in the high-order finite-element approach the potential is represented as accurately as in the dense-mesh, low-order case.

4 Nanophysics in axial symmetry

In Publications III, IV and V, we have applied the RQMG-method in various nanostructure studies. We found it convenient in all these projects to use axially symmetric model systems instead of atomistic models. This approximation reduces the computational demands and allows us to study rather large systems encompassing hundreds (Publications III and IV) and even thousands (Publication V) of electrons. In addition, by restricting the geometry to the axial symmetry and resorting to jellium models, many random effects related to the detailed and sometimes unimportant atomic structure disappear, and the relevant physics is easier to extract from the simulations.

In the axial symmetry, the Eq. (6) for the Kohn-Sham orbital

$$\psi_{m\mathbf{k}n}(\mathbf{r}) = e^{im\phi} U_{m\mathbf{k}n}(r, z) \tag{23}$$

can be replaced by the following equation

$$-\frac{1}{2}\left(\frac{1}{r}\frac{\partial}{\partial r} + \frac{\partial^2}{\partial r^2} - \frac{m^2}{r^2}\frac{\partial^2}{\partial z^2} + 2V_{eff}\right) U_{m\mathbf{k}n}(r, z) = \varepsilon_{m\mathbf{k}n} U_{m\mathbf{k}n}(r, z). \tag{24}$$

We denote the components of the **k**-vector by k_z and $k_\parallel$. The z-component k_z of the **k**-vector only has relevance in periodic systems, such as the nanowires studied in Publication IV. In the periodic case, the following Bloch boundary condition

$$U_{m\mathbf{k}n}(r, z + L_{\text{cell}}) = e^{ik_z L_{\text{cell}}} U_{m\mathbf{k}n}(r, z) \tag{25}$$

is satisfied. The radial component $k_\parallel$ enters in Publication V, where we approximate a planar system by a hexagonal lattice of circles. We see that the numerical problem is reduced to a two-dimensional one. Furthermore, the problem is conveniently split into a number of independent subproblems – the Kohn-Sham orbitals with different m or **k** are automatically orthogonal and can be solved simultaneously in a massively parallel computer environment.

4.1 Conductance oscillations in atomic chains

In Publication III, our focus has been on atomic Na chains as ultimate conductors. Monatomic Na wires consisting of more than one atom have

not been reported experimentally yet, while a possibility of the formation of three-atom-long Na wires in the breaking process of a nanocontact has been demonstrated theoretically [111] in *ab initio* molecular dynamics simulations. Following a theoretical prediction of similar atomic-scale metallic nanowires consisting of Au atoms by Sørensen *et al.* [112], such wires have actually been produced by scanning tunneling microscope (STM) [113, 114] and mechanically controllable break junction (MCBJ) technique [115]. Chains of Au atoms up to a length of 7-8 atoms have been observed to remain stable for more than an hour [116]. In addition, gold atom chains have been observed to form on stepped Si surfaces [117].

Half a century ago, Fröhlich [118] and Peierls [119] discovered an instability in one-dimensional electron systems that has come to be called the Peierls instability: the regular chain structure in a one-dimensional wire with a partly filled band will never be stable (at zero temperature), since one can always find an energetically favourable structure with a longer periodicity (e.g. doubled for a dimerized chain), for which a band gap occurs at the Fermi-level. The wire changes from metallic to insulator in this process. We do not consider the possible effects of Peierls distortions for finite Na-chains in Publication III. Note, however, the calculation by Häkkinen *et al.* [120], where a dimer is formed in the middle of a four-atom Au-chain between leads. For a recent study on Peierls instability in Al Wires, see Ref. [121].

Metallic atomic-sized contacts can be characterized by a finite set of conductance eigenchannels, each of which has its own associated transmission probability. For a point contact of just a single atom in cross section, the number of valence orbitals of the atom fixes the number of eigenchannels [122]. Thus, for monovalent metals, such as Na or Au, only a single channel contributes to the conductance.

While chains of monovalent atoms can be considered as the simplest possible conductors, their properties are not yet completely understood. Bias voltages as high as 2 V have been applied without damage to monatomic gold wires [123, 124]. With a conductance equal to $\frac{2e^2}{h}$ this corresponds to $150\mu A$, or a current density of $2 \times 10^{15} \frac{A}{m^2}$. This current density is seven orders of magnitude greater than the current density that turns the tungsten wire inside a light bulb white-hot. Such high current densities are made possible by the ballistic nature of the transport.

Different theoretical model calculations have predicted an oscillatory depen-

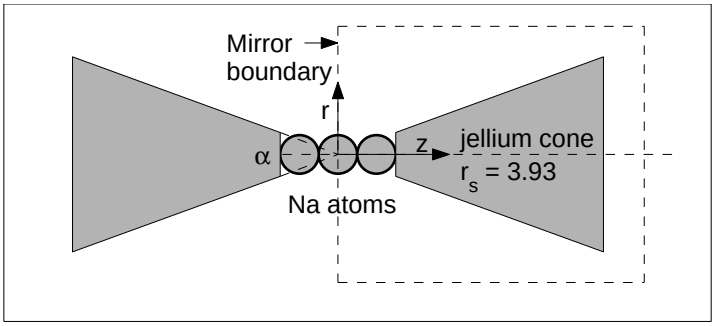

Figure 4: Geometry of the present model. Na pseudoatoms are located between two jellium cones. The cone angle α can be varied continuously. The dotted line gives the boundaries of the calculation cell.

dence of the conductance on the number of Na atoms in the chain [125–127]. In recent STM experiments of gold nanocontacts [128], a small variation of conductance within the region of a unit conductance quantum was observed (Fig. 1(a) of Ref. [128]) as the STM tip is stretched before breaking. As argued in Ref. [127], the small but abrupt jump in the conductance might originate from an addition of an extra gold atom to the chain. That is, the observed conductance variation may be a signature of the even-odd parity effects in the atomic wire.

The first reported observation of the even-odd oscillation for Au atoms appeared recently as a statistical analysis of many separate conductance measurements performed using the MCBJ technique [129]. The observed variation of the conductance was of the order of $0.01G_0$.

Our research reported in Publication III has been largely motivated by the works of Sim *et al.* [126] and Yeyati *et al.* [130]. Sim *et al.* showed that a half-filled resonance induced by a Na molecular orbital causes the high conductance for an odd number of Na atoms in the chain. For an even number of chain atoms, the resonance is filled, and below the Fermi level, which lowers the conductance. Yeyati *et al.* showed that the role of the contact leads cannot be ignored, when studying the conductance of atomic chains. To enable a systematic study of the dependence of the conductance not only on the length of the chain but also on the shape of the contacts, we replace the leads by jellium cones of finite size. The cone opening angle can be varied continuously. The geometry of our model is shown in Fig. 4.

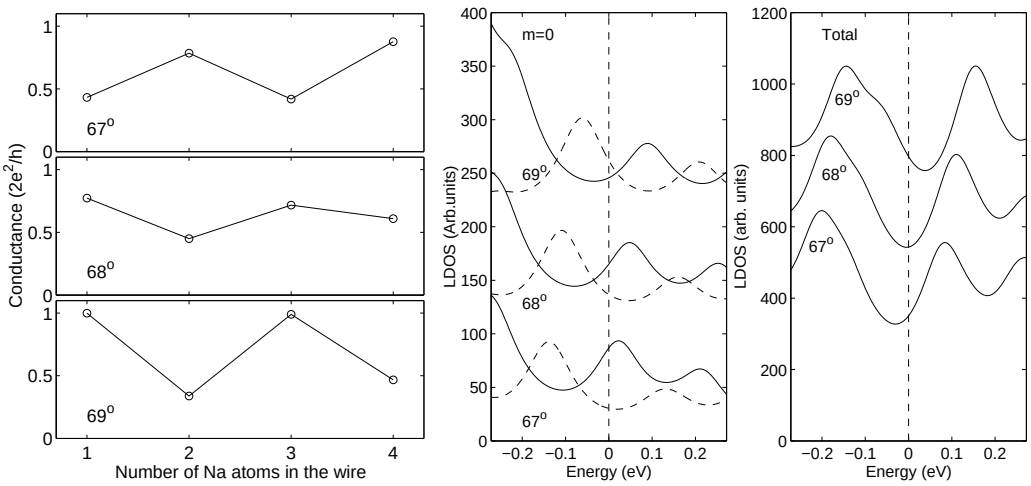

Figure 5: Left panel: Conductances of the chains of one, two, three and four Na atoms between two jellium leads. The conductances are shown for three different jellium cone angles. The number of electrons in each cone is 300. Middle and right panels: Chain of two Na atoms between two jellium leads. The local density of states (LDOS) near the Fermi level (energy zero) is given for different cone angles. The middle panel shows the even (solid line) and odd (dashed line) $m = 0$ LDOS's calculated for the atom chain between the jellium edges. The right panel shows the total LDOS's calculated for the atom chain and the tips of the leads to the depth of r_s from the jellium edge. The LDOS's corresponding to the two uppermost angles are shifted in steps of 100 and 200 units in the middle and right panels, respectively.

In the zero-bias limit, the mirror symmetry and the Friedel sum rule then give the conductance [131]

$$G = \frac{2e^2}{h} \sin^2 \left[\frac{\pi}{2} (N_e - N_o) \right], \tag{26}$$

where N_e and N_o are the numbers of electrons in the even- and odd-parity states, respectively.

As Sim *et al.* [126], we find the even-odd behaviour of the conductance as a function of the number of atoms in the chain. However, while Sim *et al.* studied atomistic leads of only one shape and found with high accuracy the conductance of 1 G_0 for an odd number of atoms, we find that the phase of the even-odd oscillation has a sensitive dependence on the shape of the leads – which in our simple model is reflected by the cone angle. This dependence

is illustrated in the left panel of Fig. 5.

The total electron density increases close to the tip as the cone angle increases. But it is important to note that the $m > 0$ electron states contribute most of the density increase. As a result, the $m = 0$ resonance states feel an increased Coulomb repulsion and are pushed upwards in energy. The shift of the $m = 0$ states towards higher energies can be seen in the LDOS integrated over the region of the chain – the volume limited by the two planes at the central jellium edges (middle panel of Fig. 5). The right panel of Fig. 5 gives the total LDOS calculated by including the tips of the cones into the integration; the limiting planes are at the depth of r_s from the central jellium edges. We see that in this volume, which is important for the charge neutrality of the atom chain, the $m = 0$ features of the left panel are hardly visible. The change of this total LDOS is also less dramatic than that of the $m = 0$ LDOS at the atom chain. On the basis of the above discussion we can conclude that the $m > 0$ states have an important contribution to the local charge neutrality and influence the conductance of the chain, even though only $m = 0$ states contribute to the single conducting channel of the system.

The finite-size effects make the interpretation of the results of our jellium calculations as well as the atomistic calculations of Sim *et al.* difficult. While we have made no attempt to mask the finite-size effects, Sim *et al.* have artificially obtained a "bulk-like" flat density of states at the Fermi level for their reference system consisting of leads only. They obtain this condition by moving the atoms slightly on the vacuum side of their lead clusters [132]. Thereby their resonance-states can couple to bulk-like states exactly at the Fermi-level, leading to half-filling and thus a conductance of 1 G_0 in the case of an odd number of atoms.

As already mentioned, in the measurements for chains of Au atoms, the last conductance plateau of about one conductance quantum is not smooth but exhibits abrupt changes synchronized with abrupt changes in the elongation force [128]. The steps in the conductance may be of the order of one tenth of the conductance quantum. Our findings give two explanations for these small conductance changes. The conductance may jump abruptly when the number of atoms in the chain increases. On the other hand, the geometry of the lead tips changes affecting also the conductance. These two effects may be superimposed during the actual elongation process.

While the Friedel sum rule of Eq. (26) is only applicable in the case of

a single conducting channel and zero bias, more sophisticated methods will be required in the future for theoretical assessing of the transport properties of molecular devices. A promising scheme for this purpose is the non-equilibrium Green's function (NEGF) technique [133] combined with self-consistent density functional calculations for the electronic structure. Using this approach, Tsukamoto and Hirose [134] have studied the electron transport properties of Na chains under applied bias voltage. A density-functional method for nonequilibrium electron transport has also been implemented within the program package TranSiesta by Brandbyge *et al.* [135]. In addition, several other groups are currently exploring NEGF-DFT approaches for transport calculations [136–141].

4.2 Jellium models for nanowires

Using remarkably simple experimental techniques it is possible to gently break a metallic contact so that during the last stages of the pulling a neck-shaped wire connects the two electrodes [116]. The diameter of the conducting nanowire is reduced down to a single atom upon further stretching. For some metals, it is even possible to form a chain of individual atoms in this fashion, as it was discussed in Sec. 4.1.

By indenting one electrode into another and then separating them in the mechanically controllable break junction (MCBJ) technique [142] or by retracting the tip of a scanning tunneling microscope (STM) [113, 128, 143] from a substrate, a stepwise decrease in the electrical conductance is observed, down to the breakpoint. A correlated oscillating decrease of the mechanical force required to pull the wire has also been observed in the STM-experiments [113]. Each scan of the dependence of conductance on the elongation is different in detail, as the atomic configuration of each contact may be different. However, statistically, many scans together produce a histogram of the probability for observing a given conductance value, which is quite reproducible for a given metal and for fixed experimental parameters. By carefully analyzing such histograms for Na nanowires, Yanson *et al.* [144–146] have observed that certain conductance values are much more probable than others. As the conductance can be related to the radius at the narrowest part of the wire, it follows, that there are magic radii with enhanced stability. These findings have been interpreted as electronic [144, 145] and atomic [146] shell structures of nanowires – in striking analogy with the corresponding shell structures observed previously in atomic

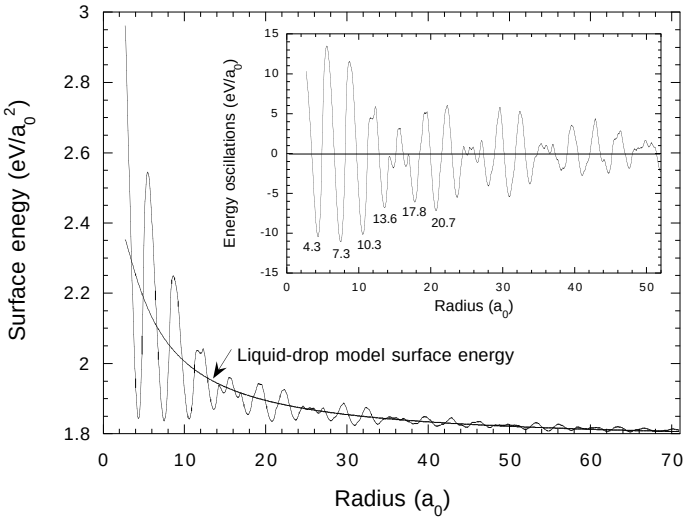

Figure 6: Surface energy of infinite uniform cylindrical UJ nanowires as a function of the nominal wire radius as defined in Publication IV. In the inset the pure oscillations of the total energy per unit length are shown and the first magic radii are marked.

clusters [147, 148].

Using a simple theoretical model [149, 150], the observed shell and supershell structures for Na have been quantitatively explained [151, 152]. In this model, the nanowires are modeled as infinite uniform stabilized jellium cylinders. The research reported in Publication IV is largely inspired by these previous studies. The aim of the paper is to simulate the breaking of nanowires. Thus the approximation of the wire as a uniform cylinder has to be abandoned. We use the ultimate jellium (UJ) model (see Sec. 2.2), previously used by Manninen *et al.* to investigate the structure of the alkali-metal clusters. To our knowledge, Publication IV is the first reported study of nanowires, where the UJ model is used.

To gain insight into the properties of the UJ-nanowires, and to relate Publication IV to the previous studies of stabilized-jellium cylinders, we first studied the stability of infinite cylindrical UJ-wires by calculating the surface energy as a function of the wire radius (Fig. 6). The pure quantum oscillations of the total energy per unit length can be seen more clearly in the inset of Fig. 6, where the average behaviour, fitted to a liquid-drop model

[153] - type function, is subtracted. The minima of this oscillating function correspond to magic radii with enhanced stability. The supershell structure, producing the periodic attenuation of the amplitude of the oscillations, can be seen as well.

Previous theoretical studies of the breaking process of nanowires can be split in two groups. The first group includes classical and *ab initio* molecular-dynamics simulations, in which the atomic structure of nanowires is taken into account. These investigations have been successful in many aspects, e.g. showing the atomistic mechanisms of the narrowing process (appearence of dislocations, order-disorder stages, etc.) and their connection to other measurable quantities such as the elongation force or the conductance [112, 154]. From the viewpoint of the results obtained in Publication IV, we notice the predictions for preferred clusterlike configurations of atoms in Na constrictions, based on atomistic *ab initio* simulations of the breaking process [154–156].

The second group of models is more related to properties due to the confinement of electrons in reduced dimensions, and ignores the atomistic and discrete structure of matter. In these calculations analytic approximations as well as self-consistent models have been used, mainly within jellium models. Whereas the first group of models tries to repeat the experiments as accurately as possible and thereby gain insight into the actual atomic processes, the second group of models tries to find the essential physics behind the phenomena seen in experiments or in atomistic simulations. The second class of methods reflect the measured average behaviour rather than individual breaking events. The methods can explain the cohesive and electronic transport properties of nanowires, especially in the case of alkali metals with strong free-electron character [151, 152, 157–160].

While Publication IV falls in the second group, it differs from methods where *ad hoc* shapes, like hyperbolic [159], parabolic [157] or cosine [160] are used for the constriction. In our model the electrons themselves acquire self-consistently the shape, which minimises the Kohn-Sham energy functional, and carry along the positive background. However, we restrict the shapes of nanowires to the axial symmetry in order to reduce computational demands and to highlight the important phenomena from the complexity of possible solutions. The freedom of the electronic structure to deform and thereby affect the ionic structure may roughly correspond to the experimental conditions at temperatures close to the melting point. Note also that in the experimental conductance histograms [144, 145] for Na, the shell

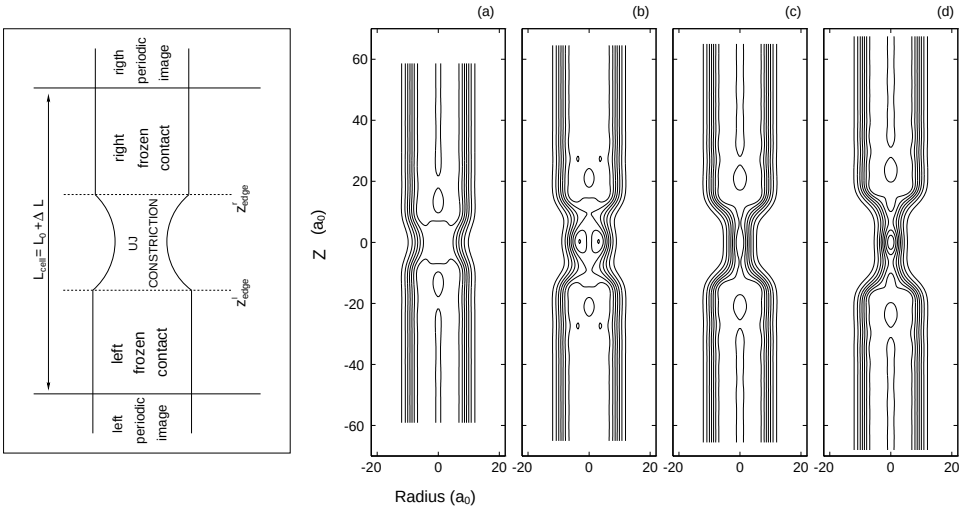

Figure 7: Left panel: Schematic view of the model system for simulations of breaking finite nanowires supported by two leads. Right panel: Supported UJ wire. The UJ constriction contains eight electrons. Density contour plots for four different elongation lengths: $\Delta L = 7.9\ a_0$ (a), $19.8\ a_0$ (b), $20.8\ a_0$ (c), and $25.8\ a_0$ (d) are shown. The snapshots in (b) and (c) are from consecutive self-consistent calculations and the snapshot (d) is the last step before the nanowire breaking.

and supershell structures are most clearly seen at the temperature of the order of 80 K. The finite temperature clarifies the quantum shell structure because the ions can rearrange to minimize the total energy.

In order to study the formation and evolution of nanoconstrictions between two supporting leads we follow the next procedure. First, we fix the number of electrons in the periodic supercell and solve self-consistently for the electronic structure of a uniform UJ wire having a stable magic radius. The uniform shape is stable due to the quantum shell structure in cylindrical geometry. Then, the potential at both ends of the periodic cell is "frozen". This means that, although the Kohn-Sham equations are solved in the whole wire, in these regions the potential is not updated in the self-consistency process. The function of this "frozen" part is to emulate the lead parts where ion rearrangement does not occur as efficiently as at the constriction. In our calculation, these leads serve as handles to grab the UJ and pull it. The rest of the wire, the UJ at the middle part of the supercell, is the place where the wire will stretch. A sketch of the configuration is shown in the

left panel of Fig. 7.

In Fig. 7(a) the electron density is shown after the elongation of $\Delta L = 7.9\ a_0$. The catenoid-like density profile appears as expected for a classical fluid. When we continue elongating the nanowire the shape of the electron density changes dramatically from the classical one.

In Fig. 7(b) $\Delta L = 19.8\ a_0$ and the electrons in the constriction form a cluster-derived structure (CDS) [154, 155]. The electron density per unit length has two minima at both sides of the CDS and there are 7.1 electrons between these narrowest cross sections. The embedded cluster resembles the spherical closed-shell cluster of eight electrons, but there are some differences. There are not enough electrons and the symmetry is not exactly spherical. The CDS, which reflects the spherical shell structure, is analyzed in detail in the paper by studying the single-particle wave functions.

Figure 7(c) shows the next consecutive elongation step with $\Delta L = 20.8\ a_0$. Note that the CDS disappears and a sudden change in the mean radius happens. In fact, the conductance changes simultaneously abruptly from 3 G_0 to 1 G_0 (see the inset in the left panel of Fig. 8). Here, we want to emphasize that the shape of the constriction is again far from the catenoid having a constant magic radius corresponding to the cylindrical shell structure. Figure 7(d) is for $\Delta L = 25.8\ a_0$, the last step before the nanowire breaks. Again a CDS appears during the elongation from the third to the fourth snapshot. There are 1.8 electrons between the two minimum cross sections at both sides of the CDS. This CDS can be interpreted as an embedded two-electron cluster. We observe that the radius of the constrictions is more or less constant with the same value as in the previous snapshot in Fig. 7(c).

The conductance, shown in the left panel of Fig. 8 is roughly estimated with the adiabatic and semiclassical approximation used by Brandbyge *et al.* [143]. The constriction is divided into transversal slices. Then for each slice a uniform wire with the z-independent effective potential of the slice is built, and the subband bottoms are calculated by solving the Schrödinger equation. The subband bottoms give effective potentials along the wire axis. To evaluate the transmission probability of the electrons at the Fermi level through the barrier at the constriction the semi-classical WKB formula is used. The elongation force, shown in the right panel of Fig. 8 is evaluated as the negative derivative of the total energy with respect to the elongation. The rearrangement of the wire charge leads to discontinuous upward steps

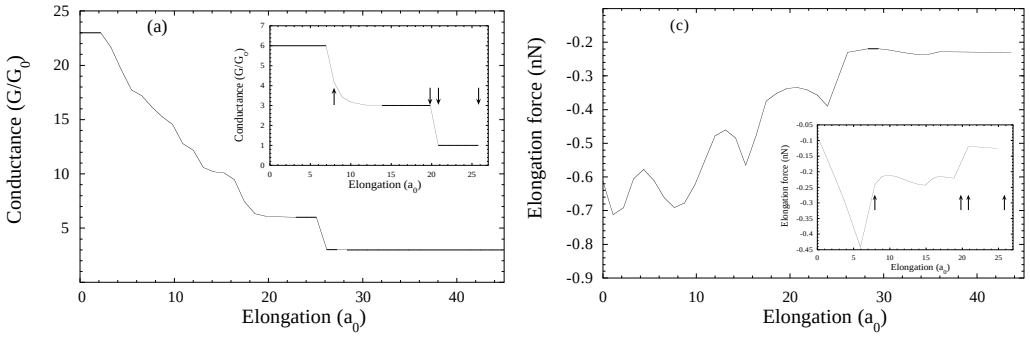

Figure 8: Main figures: conductance and elongation force for a wire with initial radius $R = 20.7\ a_0$ and about 60 UJ-electrons in the constriction. Insets: the same quantities for the wire in Fig. 7 with initial radius $R = 10\ a_0$ and 8 UJ-electrons in the constriction. The arrows mark the points were the density has been plotted in Fig. 7.

in the force, while if the radius changes smoothly the force draws a continuous buckling curve. Here, we want to point out the superiority of the UJ model in the force calculation over other jellium models [150, 157, 158]. In contrast with experiments [113, 128], the latter show a continuous oscillating behavior of the force without any steps. Moreover, for narrow constrictions positive values are obtained when the wire crosses an unstable zone. Note that in our model the force is always negative, as observed in the experiments [113, 128] and in atomistic simulations [111, 112, 143, 154]. Our results show clearly that the transport, geometrical and mechanical properties of the nanowires under elongation are related.

4.3 Adsorbed Na quantum dots on Cu(111)

Although the 4s-valence electrons in copper behave almost like free electrons, there is a bandgap in the bulk band structure projected onto the Brillouin-zone boundary along the (111) direction. When Na is deposited on the Cu(111) surface, the valence electrons induced by the adatoms are confined to the surface region by the bandgap on the substrate side and the vacuum barrier on the other side. Due to this confinement the Na valence electrons will form a two-dimensional nearly free electron gas, thus forming quantum well states. Another interesting feature is that, as indicated by recent STM measurements [161, 162], the second Na monolayer grows via

the formation of roughly hexagonal adatom islands, providing confinement also in the lateral direction for some of the quantum well states. Since these systems confine electrons in three dimensions, they are *quantum dots* (QD). Adsorbed nanostructures are interesting in order to promote or prevent specific chemical reactions, e.g. adsorption or molecular dissociation. in a controlled manner. As the local electron structure depends on atomic species and coordination (the shape of the QD), it is in principle possible to design a QD to initiate a specific reaction. An example of this new field, *nanocatalysis*, is the detailed experimental and theoretical study of the nanoscale hydrodesulfurization catalysts [163].

The usefulness of Na islands on Cu(111) as a nanocatalyst (or other purposes) can be examined, besides by experimental methods, also through computational modeling. The question arises, what level of sophistication for the computational model should be used. Since the typical Na islands include of the order of hundreds of atoms, full atomistic *ab initio* treatment of these islands on top of a Na monolayer on top of bulk copper (described e.g. as a slab of ten atomic layers, therefore implying on the order of 10^4 atoms in the supercell of a periodic system) seems intractable, although the newly introduced order-N methods [41, 65, 66, 164] are promising tools for very large scale first-principles electronic structure calculations. Free-electron model calculations have been performed for circular [165] and hexagonal [166] free-standing Na-islands. All-electron calculations for an unsupported Na monolayer [167] and plane-wave pseudopotential slab calculations for one-atomic Na layer in (2×2) and (3/2×3/2) adsorbate structures [168] on Cu(111) have been presented. As a model for Na on Cu(111), we present in Publication V self-consistent two-density-jellium calculations within the density-functional theory. The model enables the study of systems of realistic size, thereby including thousands of Na atoms.

We wish to model an isolated Na island on the top of an infinite planar Na monolayer on top of the semi-infinite copper substrate. Our first approximation is the replacement of the discrete Na atoms by a uniform positive backgound charge density with sharp boundaries (the jellium model, see Sec. 2.2). As a next step, we make the *supercell* approximation, where, instead of an isolated Na island on top of the monolayer, we treat the system as a periodic hexagonal superlattice. Finally, we replace the hexagonal unit cell of this lattice by a circle with the same area as the original hexagon as illustrated in the top left panel of Fig. 9. This approximation scheme is a two-dimensional analogue of the well known Wigner-Seitz method in solid-

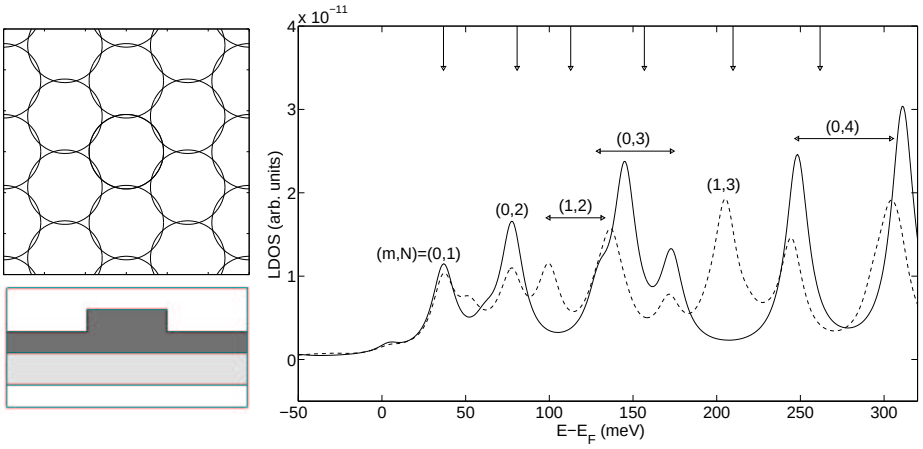

Figure 9: Top left: Hexagonal lattice of area-covering circles. Bottom left: Schematic view of the background charge density in a plane containing the z-axis in our two-density model for a quantum-dot on top of a full monolayer of Na on Cu(111) Right: Local density of states on top of a cylindrical QD of 550 electrons on two-jellium substrate.

state physics [169]. The Brillouin-zone of the lattice of circles is sampled at two **k**-points, which correspond to Kohn-Sham orbitals that are odd and even with respect to the boundary of the circle.

A schematic view of the background charge density profile in our model system is presented in the bottom left panel of Fig. 9. The essential physical effects caused by the underlying copper monolayer are captured by using a slab of lower-density jellium below the Na monolayer to mimic the decay of the surface states into the substrate. We thereby introduce two free parameters into our model – the density parameter r_{s2} and the width w_2 of the lower density slab. These parameters are fitted so that the bottoms of the two most important surface-state bands coincide with the experimental results. We have selected to fit the second band, consisting of states with one horizontal nodal plane, in the case of one monolayer coverage, and the third band (states with two horizontal nodal planes) in the case of a coverage consisting of two full monolayers. The experimental positions of these band bottoms are 0.1 eV below and above the Fermi level, respectively [170–172].

We solved the Kohn-Sham equations self-consistently using our axially symmetric implementation of the Rayleigh quotient multigrid method (Sec. 3.1). Due to the large size of the system, we encountered quite severe

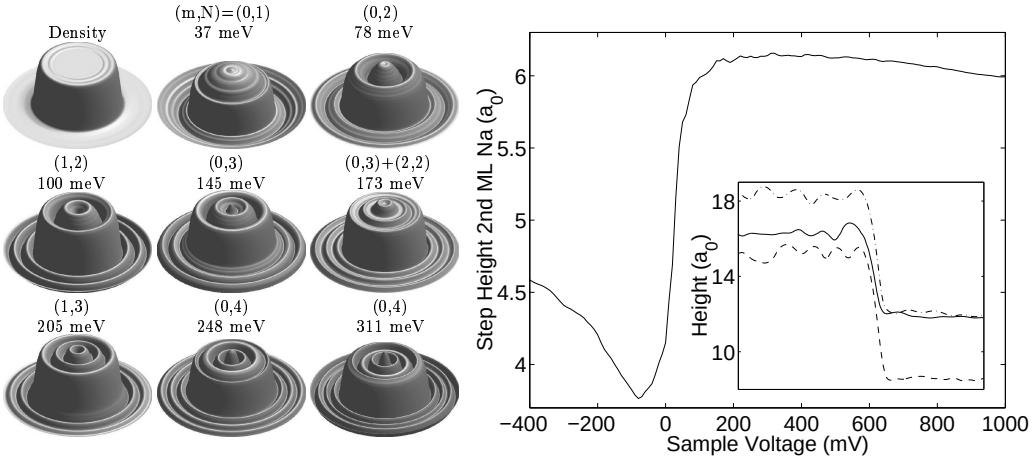

Figure 10: Left: Isosurfaces of the electron density and the LDOS at energies corresponding to the dominant peaks shown in the right panel of Fig. 9. The quantum numbers of the dominant states contributing at each energy is indicated. Right: the step height of the second Na monolayer determined from calculated constant-current surfaces (Eq. 28) is shown as a function of the bias voltage (energy relative to the Fermi level). The inset shows the LDOS isosurface profiles (height-to-radius ratio exaggerated) at energies -400 meV (dashed line) 0 meV (solid line) and 400 meV (dash-dotted line).

problems due to the well known phenomenon of charge sloshing (Sec. 3.2). In our simple model, however, the self-consistent effective potential of the large model system could be accurately estimated from the knowledge of $V_{\text{eff}}(r,z)$ for a smaller (more easily convergent) system, after which only small changes occured during the self-consistency iterations. For future calculations of this type, however, more sophisticated mixing schemes (Sec. 3.2) should be considered.

The tunneling current and differential conductance dI/dV are typical quantities measured in the STM experiments. When the applied voltage V is small, the differential conductance is proportional to local density of states (LDOS) [173, 174], which is directly available from our model calculations,

$$\frac{dI(V,r,z)}{dV} \propto \sum_{m\mathbf{kn}} (2-\delta_{0m}) |U_{m\mathbf{kn}}(r,z)|^2 \delta(\epsilon_{m\mathbf{kn}} - eV). \tag{27}$$

In our numerical calculations we replace the δ-function by a Lorenzian.

Further, we obtain a simple formula for the tunneling current,

$$I(V,r,z) = \int_0^V \frac{dI(V,r,z)}{dV} dV \propto \int_{E_F}^{E_F+eV} \rho(E,r,z) dE, \qquad (28)$$

where $\rho(E,r,z)$ is the LDOS at height z and distance r from the axis. This enables us to calculate constant-current topographs within our simple model, from which we can further extract the voltage dependence of the step height at the perimeter of the Na QD (right panel of Fig. 10).

In the STM study by Kliewer and Berndt [166], constant-current topographs and dI/dV measurements are presented for a Na island on the Na monolayer on Cu(111). The size of the island is 230×170 $a_0{}^2$ (120×90 Å^2). We have studied a cylindrical jellium dot with similar dimensions, i.e. having the radius of 85 a_0 and containing thus about 550 electrons. The Na/Cu substrate is described in our calculations by a cylindrical two-density-jellium supercell with the radius of 160 a_0 and containing 2000 electrons. We calculated the LDOS at $18a_0$ above the Na islands (right panel of Fig. 9) – a typical height in the STM dI/dV measurements. Because of the exponential decay of the Kohn-Sham orbitals into the vacuum, only those orbitals that have the slowest decay rate contribute to the LDOS at this height. These are exactly the states that have two horizontal nodal planes within the quantum-dot region e.g. the resonance states most strongly localized into the quantum dot in our model. The LDOS peaks can be labeled with the "quantum number" N by counting for the number of radial nodes of the corresponding Kohn-Sham orbital in the 2 ML part. The states strongly peaked in the QD are resonance states due to the hybridization of localized QD states with the states of the surrounding monolayer and span the whole system. Besides the delocalization of the states, the resonance character causes the fact that in the LDOS (Fig. 9) several peaks may correspond to the same resonance state. We have identified the LDOS peaks by examining the Kohn-Sham single-particle wave functions. The horizontal lines below the quantum numbers m and N connect the peaks belonging to the resonance in question.

The relative positions of the peaks appearing in the experimental dI/dV spectra by Kliewer and Berndt [166] are shown in the right panel of Fig. 9 as arrows pointing downwards. We find that our model can reproduce quantitatively the experimental peak positions. According to our calculations the resonance width increases towards higher energies. The increase is maybe

slightly stronger than in experiment, indicating somewhat too weak a confinement of the resonance states in our model.

We have also calculated the isosurfaces of the LDOS (Fig. 10) at the energies corresponding to the dominant peaks in the right panel of Fig. 9. The development of the nodal structure is clear and compares qualitatively well with that found in the experimental dI/dV maps [162]. Our results support the idea of surface states which are localized as resonances at the quantum dots. The future applications of the model will include studies of the adsorption and dissociation of molecules in the vicinity of alkali metal quantum dots. The possibility to relax the approximation of axial symmetry has been planned as well. Hexagonal (instead of cylindrical) three-dimensional jellium quantum dots can be modelled e.g. with the finite-element method (FEM) discussed briefly in Sec. 3.4. Using FEM, the sharp boundaries of the jellium system can be well represented, and coarsening the mesh in the vacuum region is straightforward. For more accurate modeling of the reaction mechanisms involving the adsorbant atom and the atoms in the QD, a cluster of atoms embedded in the jellium QD can be used. Another future direction under consideration is a fully atomistic calculation in slab geometry for reasonable-sized quantum dots, performed using the atomic orbital based, optionally linear scaling, SIESTA -code [41].

5 Summary

In this thesis, basic research focused on quantum systems relevant for the future nanotechnologies is presented. Conductance properties of chains consisting of a few Na atoms sandwiched between two metallic leads are examined. We find that the conductance depends in an oscillatory manner on the number of atoms in the chain and the shape of the contact leads has an important effect on the conductance. Cohesive and conducting properties of a breaking nanocontact are studied using a model system, which highlights the effects of the electronic structure, ignoring the evolution of the detailed ionic configuration during the breaking process. The results enlighten the physics of the phenomena seen in experiments and in atomistic simulations. Finally, a model system is developed for adsorbed Na quantum dots on the Cu(111) surface. The electronic structure arising from the model is in agreement with scanning tunneling microscope measurements. The goal is to apply this model in the future to study the reactivity of quantum dots, i.e. how different parameters as the size, shape and composition of the quantum dot may influence its ability to promote or prevent molecular dissociation or adsorption. This rather new field of surface physics is often referred to as nano-catalysis.

The computational framework for the nanostructure studies consists of the application of the Kohn-Sham scheme of the density-functional theory in axial symmetry. The axially symmetric approach is chosen, since this approximation reduces the computational demands and allows one to study rather large systems encompassing hundreds and even thousands of electrons. In addition, by restricting the geometry to the axial symmetry and resorting to jellium models, many random effects related to the detailed and sometimes unimportant atomic structure disappear, and the relevant physics is easier to extract from the simulations. In addition, it is particularly straightforward to exploit massively parallel computer architectures in the solution of the axially symmetric Kohn-Sham equations.

The Rayleigh quotient multigrid (RQMG) method developed in the work is a central ingredient in the numerical methodology used in the axially symmetric implementation of the Kohn-Sham scheme. In addition, it has been applied to the study of positron states in solids and to electronic structure calculations for quantum dots in two-dimensional electron gas. In the future, our goal is to apply real-space methods to large-scale symmetry unrestricted first-principles electronic structure calculations on a routine

basis. In a second thread of this work, several key steps towards this goal have been taken. The different applications based on the RQMG-method are collectively referred to as the MIKA-package (Multigrid Instead of the K-spAce).

During this work, the Computational Condensed Matter group (COMP) of the Laboratory of Physics of the Helsinki University of Technology and CSC – Scientific Computing Ltd. have started a collaborative project called MIKA for the development and application of real-space methods in electronic structure calculations. The author has been appointed as the project manager of the MIKA-project. The plan is to gradually expand the project through collaborations with both Finnish and foreign researchers.

Some electronic structure calculations done at CSC using the finite-element method and Krylov subspace techiques, as implemented in the ELMER-solver, developed at CSC, have already demonstrated the practicability of ELMER in electronic structure calculations. Together, ELMER and MIKA provide a good basis for further development of real-space methods for electronic structure calculations within the MIKA-project.

References

[1] W. Kohn. Rev. Mod. Phys. **71**, 1253 (1999).

[2] R. O. Jones and O. Gunnarsson. Rev. Mod. Phys. **61**, 689 (1989).

[3] S. Lundqvist and N. H. March (editors). *Theory of the Inhomogeneous Electron Gas* (Plenum Press, New York, 1983).

[4] J. F. Dobson, G. Vignale, and M. P. Das (editors). *Electronic Density Functional Theory* (Plenum Press, New York, 1998).

[5] A. Nagy. Phys. Rep. **298**, 1 (1998).

[6] L. H. Thomas. Proc. Cambridge Phil. Soc. **23**, 542 (1927).

[7] E. Fermi. Z. Phys **48**, 73 (1928).

[8] P. Hohenberg and W. Kohn. Phys. Rev. **136**, B864 (1964).

[9] M. Levy. Proc. Nat. Acad. Sci **76**, 6062 (1979).

[10] W. Kohn and L. J. Sham. Phys. Rev. **140**, A1133 (1965).

[11] D. M. Ceperley and B. J. Alder. Phys. Rev. Lett. **45**, 566 (1980).

[12] S. J. Vosko, L. Wilk, and M. Nusair. Can. J. Phys. **58**, 1200 (1980).

[13] J. P. Perdew and A. Zunger. Phys. Rev. B **23**, 5048 (1981).

[14] J. P. Perdew and Y. Wang. Phys. Rev. B **45**, 13244 (1992).

[15] J. P. Perdew and Y. Wang. Phys. Rev. B **33**, 8800 (1986).

[16] A. D. Becke. Phys. Rev. A **38**, 3098 (1988).

[17] J. P. Perdew and Y. Wang. Phys. Rev. B **33**, 8822 (1986).

[18] A. D. Becke. J. Chem. Phys. **98**, 5648 (1993).

[19] P. J. Stephens, F. J. Devlin, C. F. Chabalowski, and M. J. Frisch. J. Phys. Chem. **98**, 11623 (1994).

[20] J. Song, R. M. Ginhoven, L. R. Corrales, and H. Jonsson. Faraday Discuss. **117**, 303 (2001).

[21] J. P. Perdew, J. A. Chevary, S. H. Vosko, K. A. Jackson, M. R. Pederson, D. J. Singh, and C. Fiolhais. Phys. Rev. B **46**, 6671 (1992).

[22] J. P. Perdew, K. Burke, and M. Ernzerhof. Phys. Rev. Lett **77**, 3865 (1996).

[23] M. Ernzerhof and J. Perdew. J. Chem. Phys. **109**, 3313 (1998).

[24] H. Shore and J. Rose. Phys. Rev. B **59**, 10485 (1999).

[25] A. Kiejna. Prog. Surf. Sci. **61**, 85 (1999).

[26] J. P. Perdew, H. Q. Tran, and E. D. Smith. Phys. Rev. B **42**, 11627 (1990).

[27] H. Shore and J. Rose. Phys. Rev. Lett. **66**, 2519 (1991).

[28] M. Manninen. Phys. Rev. B. **34**, 6886 (1986).

[29] M. Koskinen, P. Lipas, and M. Manninen. Z. Phys. D **35**, 285 (1995).

[30] M. Koskinen, P. Lipas, and M. Manninen. Europhys. Lett. **30**, 519 (1995).

[31] S. M. Reimann, M. Koskinen, J. Helgesson, P. E. Lindelof, and M. Manninen. Phys. Rev. B **58**, 8111 (1998).

[32] J. Kolehmainen, H. Häkkinen, and M. Manninen. Z. Phys. D **40**, 306 (1997).

[33] R. Car and M. Parrinello. Phys. Rev. Lett. **55**, 2471 (1985).

[34] M. C. Payne, M. P. Teter, D. C. Allan, T. A. Arias, and J. D. Joannopoulos. Rev. Mod. Phys. **64**, 1045 (1992).

[35] R. N. Barnett and U. Landman. Phys. Rev. B **48**, 2081 (1993).

[36] Gaussian 03, Revision A.1, M. J. Frisch, G. W. Trucks, H. B. Schlegel, G. E. Scuseria, M. A. Robb, J. R. Cheeseman, J. A. Montgomery, Jr., T. Vreven, K. N. Kudin, J. C. Burant, J. M. Millam, S. S. Iyengar, J. Tomasi, V. Barone, B. Mennucci, M. Cossi, G. Scalmani, N. Rega, G. A. Petersson, H. Nakatsuji, M. Hada, M. Ehara, K. Toyota, R. Fukuda, J. Hasegawa, M. Ishida, T. Nakajima, Y. Honda, O. Kitao, H. Nakai, M. Klene, X. Li, J. E. Knox, H. P. Hratchian, J. B. Cross, C. Adamo, J. Jaramillo, R. Gomperts, R. E. Stratmann, O. Yazyev, A. J. Austin, R. Cammi, C. Pomelli, J. W. Ochterski, P. Y. Ayala, K. Morokuma, G. A. Voth, P. Salvador, J. J. Dannenberg, V. G. Zakrzewski, S. Dapprich, A. D. Daniels, M. C. Strain, O. Farkas, D. K. Malick, A. D. Rabuck, K. Raghavachari, J. B. Foresman, J. V. Ortiz, Q. Cui, A. G. Baboul, S. Clifford, J. Cioslowski, B. B. Stefanov, G. Liu, A. Liashenko, P. Piskorz, I. Komaromi, R. L. Martin, D. J. Fox, T. Keith, M. A. Al-Laham, C. Y. Peng, A. Nanayakkara, M. Challacombe, P. M. W. Gill, B. Johnson, W. Chen, M. W. Wong, C. Gonzalez, and J. A. Pople, Gaussian, Inc., Pittsburgh PA, 2003.

[37] B. Delley. J. Chem. Phys. **113**, 7756 (2000).

[38] G. te Velde, F. Bickelhaupt, E. Baerends, C. F. Guerra, S. van Gisbergen, J. Snijders, and T. Ziegler. J. Comput. Chem. **22**, 931 (2001).

[39] R. Ahlrichs and M. V. Arnim. In *Methods and Techniques in Computational Chemistry: METECC-95*, edited by E. Clementi and G. Corongiu (1995).

[40] High Performance Computational Chemistry Group, NWChem, A Computational Chemistry Package for Parallel Computers, Version 4.1 (2002), Pacific Northwest National Laboratory, Richland, Washington 99352, USA.

[41] J. M. Soler, E. Artacho, J. D. Gale, A. García, J. Junquera, P. Ordejón, and D. Sánchez-Portal. J. Phys. : Condens. Matter **14**, 2745 (2002).

[42] T. L. Beck. Rev. Mod. Phys. **72**, 1041 (2000).

[43] S. R. White, J. W. Wilkins, and M. P. Teter. Phys. Rev. B **39**, 5819 (1989).

[44] J. Pask, B. Klein, C. Fong, and P. Sterne. Phys. Rev. B **135**, 1 (1999).

[45] E. Tsuchida and M. Tsukada. Phys. Rev. B **52**, 5573 (1995).

[46] E. Tsuchida and M. Tsukada. J. Phys. Soc. Jap. **67**, 3844 (1998).

[47] K. Tagami, E. Tsuchida, and M. Tsukada. Surf. Sci. **446**, L108 (2000).

[48] J. R. Chelikowsky, N. Troullier, K. Wu, and Y. Saad. Phys. Rev. B **50**, 11355 (1994).

[49] A. P. Seitsonen, M. J. Puska, and R. M. Nieminen. Phys. Rev. B **51**, 14057 (1995).

[50] E. L. Briggs, D. J. Sullivan, and J. Bernholc. Phys. Rev. B **54**, 14362 (1996).

[51] F. Ancilotto, P. Blandin, and F. Toigo. Phys. Rev. B **59**, 7868 (1999).

[52] Y.-G. Jin, J.-W. Jeong, and K. Chang. Physica B **274**, 1003 (1999).

[53] J. Wang and T. L. Beck. J. Chem. Phys. **112**, 9223 (2000).

[54] U. V. Waghmare, H. Kim, I. J. Park, N. Modine, P. Maragakis, and E. Kaxiras. Comp. Phys. Comm. **137**, 341 (2001).

[55] T. A. Arias. Rev. Mod. Phys. **71**, 267 (1999).

[56] D. Bai and A. Brandt. SIAM J. Sci. Stat. Comput. **8**, 109 (1987).

[57] E. J. Bylaska, S. R. Kohn, S. B. Baden, A. Edelman, R. Kawai, M. E. G. Ong, and J. H. Weare. In *Proceedings of the 7th SIAM Conference on Parallel Processing for Scientific Computing*, edited by D. H. Bailey *et al.* (1995), p. 219.

[58] J.-L. Fattebert. J. Comput. Phys. **149**, 75 (1999).

[59] F. Gygi and G. Galli. Phys. Rev. B **52**, R2229 (1995).

[60] I. Babuska and Rheinboldt. Int. J. Num. Meth. Engng. **12**, 1579 (1978).

[61] I. Babuska and B. Szabo. Int. J. Num. Meth. Engng. **18**, 323 (1982).

[62] I. Babuska and M. Suri. Comp. Meth. Appl. Mech. Engng. **80**, 5 (1990).

[63] A. Brandt. Math. Comput. **31**, 333 (1977).

[64] A. Brandt, S. F. McCormick, and J. W. Ruge. SIAM J. Sci. Comput. (USA) **4**, 244 (1983).

[65] S. Goedecker. Rev. Mod. Phys. **71**, 1085 (1999).

[66] J.-L. Fattebert and J. Bernholc. Phys. Rev. B **62**, 1713 (2000).

[67] A. D. Becke. J. Chem. Phys **76**, 6037 (1982).

[68] A. D. Becke. Phys. Rev. A **33**, 2786 (1986).

[69] L. Laaksonen, P. Pyykkö, and D. Sundholm. Comp. Phys. Rep. **4**, 313 (1986).

[70] D. Sundholm. Comp. Phys. Comm. **49**, 409 (1988).

[71] J. Kobus, L. Laaksonen, and D. Sundholm. Comp. Phys. Comm. **98**, 346 (1996).

[72] E. L. Briggs, D. J. Sullivan, and J. Bernholc. Phys. Rev. B **52**, R5471 (1995).

[73] W. Hackbush. *Multi-Grid Methods and Applications* (Springer-Verlag, Berlin, 1985).

[74] P. Wesseling. *An Introduction to Multigrid Methods* (John Wiley & Sons, Inc., New York, 1992).

[75] W. L. Briggs, V. E. Henson, and S. F. McCormick. *A Multigrid Tutorial, Second Edition* (SIAM, 2000).

[76] T. L. Beck, K. A. Iyer, and M. P. Merrick. Int. J. Quantum Chem. **61**, 341 (1997).

[77] S. Costiner and S. Ta'asan. Phys. Rev. E **51**, 3704 (1995).

[78] S. Costiner and S. Ta'asan. Phys. Rev. E **52**, 1181 (1995).

[79] J. Wang and K. Marthinsen. Unpublished (2003).

[80] J. R. Chelikowsky, N. Troullier, and Y. Saad. Phys. Rev. Lett. **72**, 1240 (1994).

[81] X. Jing, N. Troullier, D. Dean, J. R. Chelikowsky, K. Wu, and Y. Saad. Phys. Rev. B **50**, 12234 (1994).

[82] J. R. Chelikowsky, X. Jing, K. Wu, and Y. Saad. Phys. Rev. B **53**, 12071 (1996).

[83] G. H. Golub and C. F. V. Loan. *Matrix Computations* (The Johns Hopkins University Press, London, 1989), second edition.

[84] J. Mandel and S. McCormick. J. Comput. Phys. **80**, 442 (1989).

[85] J. L. B. Cooper. Q. Appl. Math. **6**, 179 (1948).

[86] M. Manninen, R. M. Nieminen, P. Hautojärvi, and J. Arponen. Phys. Rev. B **12**, 4012 (1975).

[87] J. Arponen, P. Hautojärvi, R. M. Nieminen, and E. Pajanne. J. Phys. F **3**, 2092 (1973).

[88] R. M. Nieminen. J. Phys. F **7**, 375 (1977).

[89] G. P. Kerker. Phys. Rev. B **23**, 3082 (1981).

[90] G. Kresse and J. Furthmüller. Phys. Rev. B **54**, 11169 (1996).

[91] G. Kresse and J. Furthmüller. Comp. Mat. Sci. **6**, 15 (1996).

[92] D. R. Bowler and M. J. Gillan. Chem. Phys. Lett. **325**, 473 (2000).

[93] D. Rackowski, A.Canning, and L. W. Wang. Phys. Rev. B **64**, 121101 (2001).

[94] H. Saarikoski, E. Räsänen, S. Siljamäki, A. Harju, M. Puska, and R. Nieminen. Eur. Phys. J. B **26**, 241 (2002).

[95] E. Räsänen, H. Saarikoski, M. J. Puska, and R. M. Nieminen. Phys. Rev. B **67**, 035326 (2003).

[96] H. Saarikoski, M. J. Puska, and R. M. Nieminen. Int. J. Quantum Chem. **91**, 490 (2003).

[97] M. J. Puska and R. M. Nieminen. Rev. Mod. Phys. **66**, 841 (1994).

[98] K. Engström, J. Kinaret, R. Shekhter, M. J. Puska, and H. Saarikoski. Low Temp. Phys. (in print) (2003).

[99] S. Riikonen, T. Torsti, M. J. Puska, and R. M. Nieminen. Unpublished (2002).

[100] T. Ono and K. Hirose. Phys. Rev. Lett. **82**, 5016 (1999).

[101] R. Feynman. Phys. Rev. **56**, 340 (1939).

[102] W. H. Press, B. P. Flannery, S. A. Teukolsky, and W. T. Vetterling. *Numerical Recipes: The Art of Scientific Computing* (Cambridge University Press, Cambridge, 1989). Fortran version.

[103] C. G. Broyden. J. Inst. Math. Appl. **6**, 222 (1970).

[104] R. Fletcher. Comp. J. **13**, 317 (1970).

[105] D. Goldfarb. Math. Comput. **24**, 23 (1970).

[106] D. F. Shanno. Math. Comput. **24**, 647 (1970).

[107] M. I. J. Probert and M. C. Payne. Phys. Rev. B **67**, 075204 (2003).

[108] C. Johnsson. *Numerical Solution of Partial Differential Equations by the Finite Element Method* (Studentlitteratur, 1987).

[109] D. Braess. *Finite Elements. Theory, Fast Solvers and Applications in Solid Mechanics* (Cambridge University Press, 2001).

[110] Y. Saad. *Numerical Methods for Large Eigenvalue Problems* (Manchester University Press, Manchester, 1992).

[111] A. Nakamura, M. Brandbyge, L. B. Hansen, and K. W. Jacobsen. Phys. Rev. Lett. **82**, 1538 (1999).

[112] M. R. Sørensen, M. Brandbyge, and K. W. Jacobsen. Phys. Rev. B **57**, 3283 (1998).

[113] G. Rubio, N. Agraït, and S. Vieira. Phys. Rev. Lett. **76**, 2302 (1996).

[114] H. Ohnishi, Y. Kondo, and K. Takayanagi. Nature **395**, 780 (1998).

[115] A. I. Yanson, G. Rubio-Bollinger, H. E. van den Brom, N. Agraït, and J. M. van Ruitenbeek. Nature **395**, 783 (1998).

[116] N. Agraït, A. L. Yeayati, and J. M. van Ruitenbeek. Phys. Rep. (to be published); eprint cond-mat/0208239.

[117] P. Segovia, D. Purdle, M. Hengsberger, and Y. Baer. Nature **402**, 504 (1999).

[118] H. Fröhlich. Proc. Roy. Soc. A **223**, 296 (1954).

[119] R. E. Peierls. *Quantum Theory of Solid* (Oxford University Press, London, 1955).

[120] H. Häkkinen, R. N. Barnett, and U. Landman. J. Phys. Chem. **103**, 8814 (1999).

[121] T. Ono and K. Hirose. preprint cond-mat/0212603 (2003).

[122] E. Scheer, N. Agraït, J. C. Cuevas, A. L. Yeyati, B. Ludolph, A. Martín-Rodero, G. Rubio-Bollinger, J. M. van Ruitenbeek, and C. Urbina. Nature **394**, 154 (1998).

[123] C. Untiedt, G. Rubio-Bollinger, S. Vieira, and N. Agraït. Phys. Rev. B **62**, 9962 (2000).

[124] S. Nielsen, M. Brandbyge, K. Hansen, K. Stokbro, J. van Ruitenbeek, and F. Besenbacher. Phys. Rev. Lett. **89**, 066804 (2002).

[125] N. D. Lang. Phys. Rev. Lett. **79**, 1357 (1997).

[126] H.-S. Sim, H.-W. Lee, and K. J. Chang. Phys. Rev. Lett. **87**, 096803 (2001).

[127] T.-S. Kim and S. Hershfield. Phys. Rev. B **65**, 214526 (2002).

[128] G. Rubio-Bollinger, S. R. Bahn, N. Agrait, K. W. Jacobsen, and S. Vieira. Phys. Rev. Lett. **87**, 026101 (2001).

[129] R. H. M. Smit, C. Untiedt, G. Rubio-Bollinger, and J. M. van Ruitenbeek. In *Proceedings of Trends in Nanotechnology*, edited by A. Correia *et al.* (2002), p. 493.

[130] A. L. Yeyati, A. Martín-Rodero, and F. Flores. Phys. Rev. B **56**, 10369 (1997).

[131] S. Datta and W. Tian. Phys. Rev. B **55**, R1914 (1997).

[132] H.-S. Sim and H.-W. Lee. Private communication (2002).

[133] S. Datta. *Electronic Transport in Mesoscopic Systems* (Cambridge University Press, Cambridge, 1995).

[134] S. Tsukamoto and K. Hirose. Phys. Rev. B **66**, 161402 (2002).

[135] M. Brandbyge, J.-L. Mozos, P. Ordejón, J. Taylor, and K. Stokbro. Phys. Rev. B **65**, 165401 (2002).

[136] Y. Q. Xue, S. Datta, and M. A. Ratner. Chem. Phys. **281**, 151 (2002).

[137] M. D. Ventra and N. D. Lang. Phys. Rev. B **65**, 045402 (2002).

[138] J. Taylor, H. Guo, and J. Wang. Phys. Rev. B **63**, 245407 (2001).

[139] M. B. Nardelli, J.-L. Fattebert, and J. Bernholc. Phys. Rev. B **64**, 245423 (2001).

[140] J. Heurich, J. C. Cuevas, W. Wenzel, and G. Schön. Phys. Rev. Lett. **88**, 256803 (2002).

[141] P. S. Damle, A. W. Ghosh, and S. Datta. Phys. Rev. B **64**, 201403(R) (2001).

[142] J. M. Krans, J. M. van Ruitenbeek, V. V. Fisun, I. K. Yanson, and L. J. de Jongh. Nature **375**, 767 (1995).

[143] M. Brandbyge, J. Schiøtz, P. Stoltze, K. Jacobsen, and J. Nørskov. Phys. Rev. B **52**, 8499 (1995).

[144] A. I. Yanson, I. K. Yanson, and J. M. van Ruitenbeek. Nature **400**, 144 (1999).

[145] A. I. Yanson, I. K. Yanson, and J. M. van Ruitenbeek. Phys. Rev. Lett. **84**, 5832 (2000).

[146] A. Yanson, I. Yanson, and J. van Ruitenbeek. Phys. Rev. Lett. **87**, 216805 (2001).

[147] M. Brack. Rev. Mod. Phys. **65**, 677 (1993).

[148] W. A. de Heer. Rev. Mod. Phys. **65**, 611 (1993).

[149] N. Zabala, M. J. Puska, and R. M. Nieminen. Phys. Rev. Lett. **80**, 3336 (1998).

[150] N. Zabala, M. J. Puska, and R. M. Nieminen. Phys. Rev. B **59**, 12652 (1999).

[151] M. Puska, E. Ogando, and N. Zabala. Phys. Rev. B. **64**, 033401 (2001).

[152] E. Ogando, N. Zabala, and M. Puska. Nanotechnology **13**, 363 (2002).

[153] P. Ziesche, M. J. Puska, T. Korhonen, and R. M. Nieminen. J. Phys.: Condens. Matter **5**, 9049 (1993).

[154] U. Landman. Solid State Commun. **107**, 693 (1998).

[155] R. N. Barnett and U. Landman. Nature **387**, 788 (1997).

[156] H. Häkkinen and M. Manninen. Europhys. Lett. **44**, 80 (1998).

[157] C. Yannouleas, E. N. Bogachek, and U. Landman. Phys. Rev. B **57**, 4872 (1998).

[158] C. Yannouleas and U. Landman. J. Phys. Chem. B **101**, 5780 (1997).

[159] J. A. Torres, J. I. Pascual, and J. J. Sáenz. Phys. Rev. B **49**, 16581 (1994).

[160] C. A. Stafford, D. Baeriswyl, and J. Bürki. Phys. Rev. Lett. **79**, 2863 (1997).

[161] J. Kliewer and R. Berndt. Surf. Sci. **477**, 250 (2001).

[162] J. Kliewer and R. Berndt. Phys. Rev. B **65**, 035412 (2001).

[163] J. V. Lauritsen, S. Helveg, E. Lægsgaard, I. Stengaard, B. S. Clausen, H. Topsø, and F. Besenbacher. J. Catal. **197**, 1 (2001).

[164] D. R. Bowler, T. Miyazaki, and M. J. Gillan. J.Phys.: Condens. Matter **14**, 2781 (2002).

[165] V. Lindberg and B. Hellsing. Surf. Sci. **506**, 297 (2002).

[166] J. Kliewer and R. Berndt. Appl. Phys. A: Mater. Sci. Process **A72**, S155 (2001).

[167] E. Wimmer. J. Phys. F. **13**, 2313 (1983).

[168] B. Hellsing, J. Carlsson, L. Walldén, and S. Å. Lindgren. Phys. Rev. B **61**, 2343 (2000).

[169] C. Kittel. *Introduction to Solid State Physics*, 7th ed. (Wiley, New York, 1996), pp. 248–252.

[170] N. Fischer, S. Schuppler, R. Fischer, T. Fauster, and W. Steinmann. Phys. Rev. B **43**, 14722 (1991).

[171] S.-Å. Lindgren and L. Walldén. Phys. Rev. B **38**, 3060 (1988).

[172] A. Carlsson, S.-Å. Lindgren, C. Svensson, and L. Walldén. Phys. Rev. B **50**, 8926 (1994).

[173] A. Selloni, P. Carnevali, E. Tosatti, and C. D. Chen. Phys. Rev. B **31**, 2602 (1985).

[174] J. Li, W.-D. Schneider, and R. Berndt. Phys. Rev. B **56**, 7656 (1997).